RESONANCE POSITION AND FULL WIDTH HALF MAXIMUM IN LSMO THIN FILM USING FMR TECHNIQUE

By

Godfred Inkoom BSc. PHYSICS (Hons.)

A Thesis Submitted to the Department of Physics, Kwame Nkrumah University of Science and Technology in partial fulfillment of the requirement for a degree of

MASTER OF SCIENCE (SOLID STATE PHYSICS)

Faculty of Physical Science

College of Science

July 2011

DECLARATION

I hereby declare that this submission is my own work towards the MSc degree and that to my best of knowledge, it contains no material previously published by another person nor material which has been accepted for the award of any other degree of the University, except where due acknowledgement has been made in the text.

GODRFED INKOOM (PG 1539407)

…….....	……	…….
Student Name and ID	Signature	Date

Certified by:

PROF F. BOAKYE

…….. …	……..	……..
Supervisor	Signature	Date

Certified by:

PROF. S.K. DANOUR

……..	……..……	…….
Head of Department	Signature	Date

ACKNOWLEDGEMENT

The Lord has been good to me and so Him alone deserves my glory and thanks and for all that He has done, especially for His mercies and strength which has enabled me to complete this work.

I am most grateful to my supervisor Prof. F. Boakye for his guidance and support when things were not going on well as expected, as well as Prof R.K. Nkum, the Provost of College of Science, KNUST.

I am also grateful to my mentor, Dr. M.J. Eghan at the Department of Physics, University of Cape Coast for his valuable and immense support.

My thanks go to all my colleagues especially Michael Edem Donkoh (PhD), Asmund (PhD student at NTNU) and Justice Archer for their advice and contributions towards the completion of this work.

Finally, my sincere thanks go to my family members especially my mom Miss Janet Nyame, Mrs Ivy Asare Bediako, Samuel Adutwum, Barbara Addo, Augustina Anane and Theophilus Incoom for their support and encouragement throughout the period of my studies.

DEDICATION

I dedicate this work to my sweet mother Miss Janet Nyame and my late father Mr. Raymond Incoom

ABSTRACT

This thesis determines the temperature dependence of the FMR spectra, the angular dependence of the FMR signal and the magnetic property (resonance position and full width half maximum) of the resonance field of a 15 uc thick LSMO thin film sample on a single crystalline $SrTiO_3$ (STO) substrate at 150 K and 9.75 GHz using ferromagnetic resonance (FMR) technique. It was observed from the plot of the recorded signal versus the field (FMR spectra) at various temperatures (150 K, 200 K and 250 K) that as the temperature increases, the FMR spectra shifts to higher fields and this might be as a result of transition into the ferromagnetic state. The angular dependence of the FMR signal showed complicated phenomena at all temperatures and this might be due to the shape effects and other contributing factors such as misfit strain and crystal misfit in the LSMO thin film as discussed by other report. A plot of the resonance field versus the in-plane angle (when magnetic field is applied parallel to the thin film) showed a spectrum which was sinusoidal-like in nature with maximum and minimum curvatures. The resonance position and the full width half maximum (FWHM) of the 15 uc thick LSMO thin film sample were 1070.1875 Oe and 159.3125 Oe respectively. Ferromagnetic resonance (FMR) has also been observed in various unit cells of LSMO thin film for both simple width and simple position at 150 K and this observation of FMR has been used to confirm in-plane anisotropy of magnetic properties of LSMO/STO substrate which is as a result of distribution of anisotropies in the film. The 15 uc thick LSMO thin film displayed ferromagnetic resonance at 200 K and 250 K and this has also been confirmed by the surface plots.

TABLE OF CONTENTS

CHAPTER ONE

CHAPTER THREE

CHAPTER FOUR

CHAPTER FIVE

CHAPTER SIX

CHAPTER SEVEN

LIST OF FIGURES

FIGURE **PAGE**

LIST OF TABLE

TABLE **PAGE**

ABBREVIATIONS AND ACRONYMS

LSMO $La_{0.7}Sr_{0.3}MnO_3$

FMR Ferromagnetic resonance

Q	Quality factor
CMR	Colossal magnetoresistance
T_C	Curie temperature
ρ	Resistivity
r_A	Ionic radius of an atom
σ	Conductivity
h	Planck's constant
a_o	Lattice constant
AF	Antiferromagnetic
F	Ferromagnetic
H_R	Resonance field
J_l	Exchange interaction
M_S	Saturation magnetization
ΔH	Ferromagnetic resonance linewidth
χ	Susceptibility tensor
f	Frequency
g	Gyromagnetic ratio
M	Magnetization
MAE	Magnetocrytalline anisotropy energy
E_F	Fermi energy
ω_o	Larmor frequency
μ	Magnetic dipole moment
H	Magnetic field
EPR	Electron paramagnetic resonance
H_{eff}	Effective field

Θ and γ	Magnetization angles
ΔH_o	Inhomogeneous contribution to linewidth
TMS	Two magnon scattering
H_d	Demagntization field
P	Microwave power
χ_{rf}	rf magnetic field
d_{ex}	Exchange length
A	Exchange stiffness constant
PMA	Perpendicular magnetic anisotropy
ξ	Spin –orbit coupling parameter
L	Orbital angular momentum operator
S	Spin angular momentum operator
E_{ani}	Energy density
H_{ani}	Anisotropy field
K_S	Shape anisotropy
E_{str}	Stray field energy
F	Free energy density
S	Entropy
W	Workdone
T	Temperature
E_{cry}	Magnetocrystalline energy per unit volume
TOM	Torsion oscillation magnetometry
K^{eff}	Effective anisotropy constant
uc	unit cell
STO	$SrTiO_3$

CHAPTER ONE

1.0 INTRODUCTION

1.1 BRIEF HISTORY OF FERROMAGNETIC RESONANCE

The phenomenon of ferromagnetic resonance (FMR) was discovered originally by Griffiths (1946) but the theory of the resonance effect was proposed by Kittel (Kittel, 1948). In the research work which was conducted by Griffiths, he measured the variation of the quality factor, Q of a microwave cavity which had a ferromagnetic material electroplated on one end wall and a variable magnetic field was applied across it (Farle, 1998).

The main outcome of the theory which was proposed by Kittel was that, instead of the Larmor condition which is expressed as

The manganites are a group of compounds with a chemical formula

is

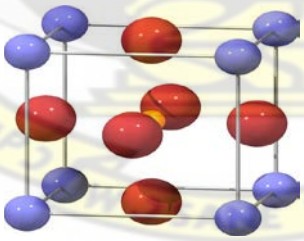

Theoretically, there is a direct relation between the conductivity and ferromagnetism. This relation is expressed as:

structure accommodates misfits in the ionic sizes and electronically induced deformations by various kinds of distortion to larger cells with lower symmetry (Coey et al., 1999).

Historically, the mixed –valence perovskites,

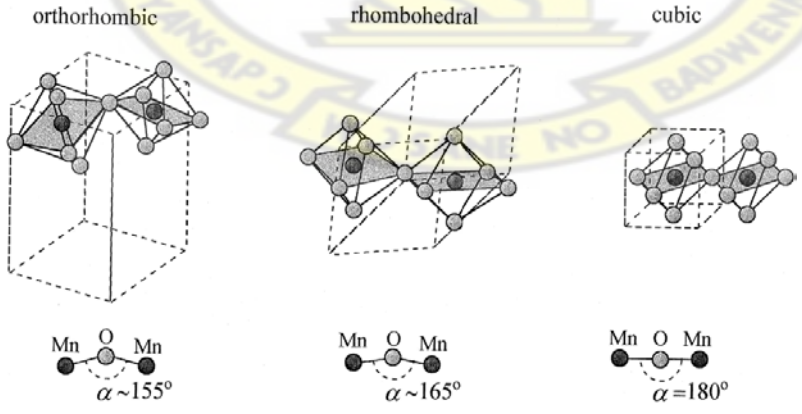

Figure 1.2: The schematic drawing of the arrangement of MnO_6 octahedra in orthorhombic, rhombohedral and (pseudo) cubic LSMO lattices. Dashed lines correspond to the unit cell of each lattice (Manabe et al., 1998).

Typical structural study of

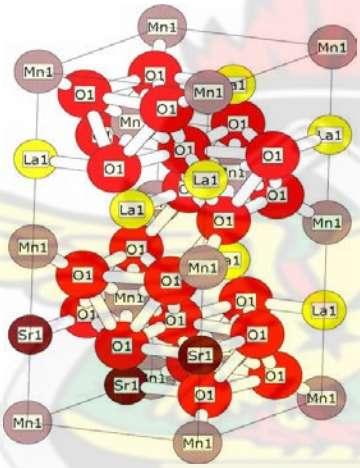

1.1.3 SOME TECHNIQUES OF FABRICATING LSMO AND MANGANITE THIN FILMS

There are several techniques which are used for fabricating thin films. Some of these thin films fabrication techniques include; sol-gel dip coating, molecular beam epitaxy (MBE), pulsed laser deposition (PLD), metal organic chemical vapour deposition (MOCVP), sputtering, cathodic arc deposition, electrohydrodynamics deposition, atomic layer deposition (ALD) and spray pyroysis. But the pulsed laser deposition (PLD) technique from sintered ceramic target has mainly been used for the growth of the manganites thin films (Coey et al., 1999).

For pulsed laser deposition technique, critical factors such as the atmosphere in the chamber and the temperature of the substrate are very critical for the growth of high quality thin films (Coey et al., 1999). For example, by using an oxygen pressure of $10 - 50$ Pa and a substrate of MgO, $SrTiO_3$ (STO) or $LaAlO_3$ (LAO) which has been heated to about $600 - 800\ ^0C$, good quality films have been grown (Coey et al., 1999). This technique has been used to grow quality thin films such as $La_{0.7}Sr_{0.3}MnO_3$, $La_{0.67}Bd_{0.33}MnO_3$ and $La_{0.7}Ca_{0.3}MnO_3$. The pulsed laser deposition (PLD) technique can be used in growing thin films of the order 100 nm or less but the molecular beam epitaxial technique is mainly used to grow highest quality films (Coey et al., 1999). One of the disadvantages of the pulsed laser deposition technique is the tendency for the micrometer-size droplets which are ejected from the target to litter the growing film (Coey, 2010). This barrier can be overcome by working at an energy density which is close to the ablation threshold by using fully dense target (Coey, 2010). The ablation threshold which is a material and wavelength dependent property is defined as the minimum fluence in which the expulsion of a given material in the form of hot plasma is obtained (Coey, 2010). Although the pulsed laser deposition(PLD) technique is used in growing quality thin films, the magnetron

sputtering technique is more preferable than the PLD technique as a result of its compatibility with current existing large scale integrating (LSI) processes (Uemura et al., 2005).

In molecular beam epitaxy, the pressure of the evaporating species is usually in the range 10^6 – 10^4 Pa. During the molecular beam epitaxy process in the fabrication of thin films, sometimes the atoms from the evaporation source are scattered before they get to the substrate (Coey, 2010). In order to overcome this barrier, the mean free path of the emitted atoms from the evaporation source must be greater than the size of the chamber. The technique of electrochemistry can also be used in growing thin films of the manganites. During this process, $LaMnO_3$ is deposited unto $SrTiO_3$ substrate from a 1M solution of lanthanum and manganese nitrate under ultraviolet illumination (Coey et al., 1999).

There are several oxide materials with perovskite structure which can be used as substrate for high epitaxial growth of LSMO thin films but $SrTiO_3$ (STO) and $LaAlO_3$ (LAO) substrates are mainly used for growing quality films as a result of the small misfits which emerge after the fabrication process (Kim et al., 2006). This is because the lattice constant of STO, a_{STO} = 0.391 nm and LAO, a_{LAO} = 0.380 nm are comparable to the lattice constant of LSMO, a_{LSMO} = 0.388 nm at room temperature (Coey et al., 1999). In the case of LSMO thin film which is fabricated on STO substrate, one can observe a misfit strain, m = 0.007732 at room temperature (Farag et al., 2005). For LSMO thin film which is fabricated on LAO substrate, an in-plane compressive strain of -0.021 can be observed. Some other substrates which can be used in fabricating LSMO thin films using the technique of pulsed laser deposition (PLD) are ZnO, MgO, $NdGaO_3$, $LaGaO_3$ (LGO) and Al_2O_3(AO) . It can be observed from the above that most of the LSMO thin films are deposited onto oxide substrates by pulsed laser deposition technique (Uemura et al., 2005). This is done so that the effect of lattice mismatch can be minimized (Kim et al., 2006).

In order to achieve good quality colossal mangnetoresistant manganites (CMR) thin films such as LSMO, there are other two materials properties of CMR film and the substrate that are very critical apart from lattice mismatch. These are chemical reaction and different thermal expansion. The difference in the thermal expansion coefficients between the thin films of the oxide and the substrate results in a structural phase transformations (Kim et al., 2006). Thin film of LSMO which is fabricated on most substrate results in strain and the presence of strain can be attributed to the difference in crystal structure between the film and the substrate (Farag et al., 2005). It has been established that thin film properties of the manganite perovskites such as LSMO, LCMO and LBMO are not only affected by lattice misfit but also by annealing conditions, layer thickness, and mechanism of strain relaxation (Liu et al., 2005). It has also been established recently that the deposition of Au on top of a 4 nm thick LSMO film results in a drastic reduction in the Curie temperature to 188 K with respect to an uncoated LSMO thin films of the same thickness (Brivio et al., 2010). Recent studies have shown that the magnetic and transport properties of the thin films of the CMR materials can be improved by postannealing in oxygen. This improvement in the magnetic and transport properties can be attributed to the oxygen incorporation which transforms Mn^{3+} ions to Mn^{4+} with smaller ionic radii and which induces the changes in the unit-cell volume (Seo et al., 2005). Research on the effect of tensile strain on LSMO thin films has also shown a reduction in the Curie temperature and this anomaly was successfully explained using the idea of double exchange interaction (Ma et al., 2006).

1.1.4 FERROMAGNETIC RESONANCE (FMR) AND FERROMAGNETIC RESONANCE LINEWIDTH

Ferromagnetic resonance (FMR) is a primary technique which is used for the study of the forces that determine the dynamical properties of magnetic materials (Sankey et al., 2006).

Ferromagnetic resonance (FMR) is a classical and a well established technique with a solid theoretical background which can be used for the interpretation of experimental spectra (Farle, 1998). Ferromagnetic resonance studies are probably the most sensitive method for detecting ferromagnetic order as well as the possible existence of other magnetic species. With ferromagnetic resonance (FMR) and electron paramagnetic resonance (EPR), a total of

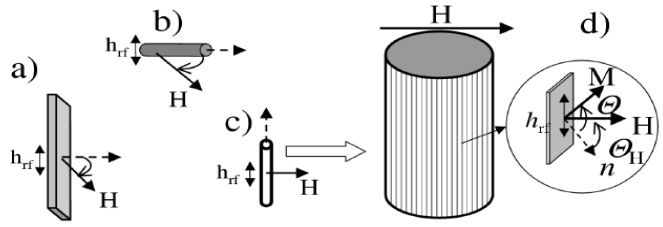

Figure 1.4: Schematic drawings of the magnetic field configuration used in FMR measurements of thin film (a), magnetic wire (b), and thin film tubes (c). Thin film tube divided into a large number of ribbons (d). Each ribbon is approximated by a thin film (Dubowik and Gos´cian´ska, 2008)

In discussing ferromagnetic resonance, it is sometimes useful to think in terms of spin waves. Spin waves are the excitations that exist in magnetic materials, the analog for magnetically ordered systems of lattice waves in solid states (Stancil and Prabhakar, 2009) and are also the fundamental dynamic magnetic excitations in ferromagnets (Covington et al., 2003). Theoretically, the prediction of spin waves resonance in ferromagnetic thin film was expressed by Kittel in a manner that predicts the computation of real and imaginary parts of the circularly polarized RF fields as well as the power absorption spectrum (Hartwell, 1968). In most of these theoretical studies, it is assumed that the Hamiltonian includes the exchange interactions between the nearest-neighbouring spins (nn exchange model). In ferromagnets, the spins are coupled by both nearest-neighbour and next-nearest-neighbour (nnn) exchange interactions

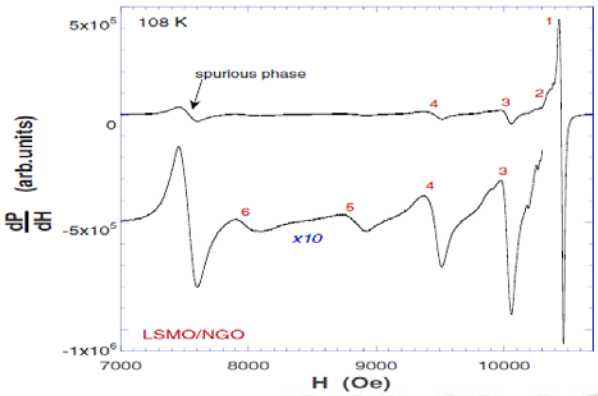

Figure 1.5: FMR spectra for a 200 nm thick $La_{0.7}Sr_{0.3}MnO_3$ film on the $SrTiO_3$ substrate in a perpendicular plane at a microwave frequency of 9.40 GHz and a modulation field of 10 Oe (Golosovsky et al., 2007)

A typical ferromagnetic resonance experiment consists of irradiating a ferromagnetic sample in an applied field with microwaves of fixed frequency where the magnitude of the applied field is varied and the energy absorbed by the sample as a function of the field is measured. When the applied field satisfies the resonance condition the energy absorbed by the sample becomes a maximum. Quantities such as the g-factor, the saturation magnetization

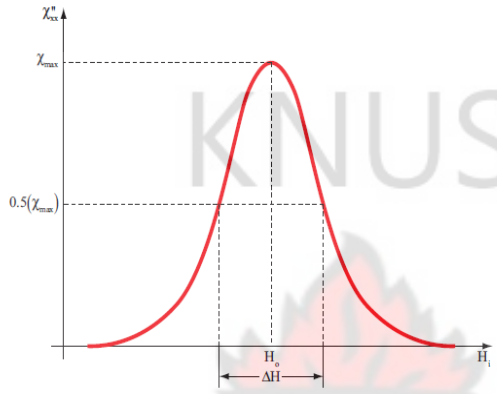

magnetization losing its energy and approaching equilibrium in magnetic materials (McMichael et al., 2004).

1.1.5 SOME ADVANTAGES OF FMR TECHNIQUE

The technique of ferromagnetic resonance has several advantages. Some of these advantages are (Farle, 1998):

(a) High sensitivity, the FMR-signal of 10^{10} – 10^{14} magnetic moments (ferromagnetically ordered) can be measured in a matter of minutes

(b) High resolution, shifts in the resonance field of a few Oersteds is easily detected. This corresponds to an energy resolution in the determination of magnetic anisotropy on the order of 0.1 eV. Second-, fourth-, and sixth-order anisotropy coefficients have been measured.

(c) Ground-state properties are measured. Only the lowest energy spin waves (wave vector

(e) In principle, a local probe which measures the internal effective magnetic field at a given site, lateral resolution can be achieved on a micrometer scale.

(f) Relaxation times of the magnetization on the order of 10^{-7} –10^{-10} s can be measured. This is also the time window in which the magnetic response is obtained.

(g) Easy set-up, all equipment is standard and readily available.

1.1.6 FMR LINE INTENSITY AND FILM MAGNETIZATION

Theoretically, it has been observed that ferromagnetic resonance (FMR) does not measure the magnetocrystalline anisotropy energy (MAE) but rather the ratio of magnetocrystalline anisotropy energy (MAE) to the magnetization (M) (Farle, 1998). The magnetocrystalline anisotropy energy (MAE), is the type of energy that directs the magnetization along a certain crystallographic axis, normally called the easy axis. It is such a very small quantity which is a few

(Farle, 1998). In most cases, the absolute determination of the total magnetic moment from the FMR signal is difficult and this requires knowledge of the microwave bridge parameter (Farle, 1998). However, a relative determination of the total magnetic moment as a function of temperature is simple due to the fact that the sample position within the microwave cavity does not change during the measurement (Farle, 1998). The microwave bridge of an EPR spectrometer houses the microwave source and the detector which is used in the FMR experiment (Jiang and Weber, 2001). The high sensitivity of the magnetic resonance technique is capable of measuring the magnetic response even on the paramagnetic side of Curie temperature,

1.1.7 SOME POTENTIAL APPLICATIONS OF THE MANGANITES AND LSMO

With the discovery of the mixed-valence manganites, numerous applications are being anticipated for but these numerous and potential applications are based on the chemical and physical properties (Coey et al., 1999) and also on some other rich properties such as colossal magnetoresistance, half-metallic ferromagnetism, magnetism of the oxides in semiconductors with doping level and an electrically driven reversible resistance switching (Mattews et al., 2009). Thin films from these mixed-valence manganites may be used as sensors and in the chemical industry also it can also be applied in catalysis (Coey et al., 1999). In this area of chemical application, it is believed that the mixed-valence manganites can be used as catalysts for automobile exhausts, oxygen sensors and solid electrolytes in fuel cells (Coey et al., 1999). In the area of magnetoresistance, it is believed that the mixed-valence manganites can be applied in areas including magnetic sensors, magnetoresistive read heads and magnetoresistive random access memory (Coey et al., 1999).

LSMO which is the most researched and studied colossal magnetoresistant manganite offers a good choice for ferromagnetic layers in magnetic tunnel junctions and other spin-injection devices such as spin valves especially when it is grown on STO and NGO as a result of the fact that this special class of the mixed-valence manganites has nearly

It should also be mentioned that this same material,

1.3 RESEARCH OBJECTIVES

The purpose of this research work is to determine the magnetic property (resonance position and full width half-maximum) of the resonance field of a 15 unit cell (uc) thick

In the third chapter, the methodology adopted in this work will be discussed. Some issues to be addressed include; sample preparation and the Bruker Elexsys E500 EPR spectrometer and the experimental procedure.

The result and discussion of the outcome of the experimental work will be given in detail in the fourth chapter. The conclusion and recommendations derived from the results are outlined in the fifth chapter. This chapter is then followed by the references and appendices.

CHAPTER TWO

2.0 LITERATURE REVIEW

2.1 MAGNETIZATION DYNAMICS

Magnetic systems are usually characterized by equilibrium or a metastable magnetic state and this corresponds to a global respective local minimum of the total energy of the magnetic systems (Stanescu, 2004). The transition of the magnetization from one state to another under the influence of an external magnetic field, temperature or a spin polarized current is called magnetization dynamics (Stanescu, 2004). Generally, magnetization processes are time-dependent even if the external magnetic field is kept constant (Sellmyer and Skomski, 2006). For instance, freshly magnetized permanent magnets lose a small fraction of its magnetization during the first few hours whiles in the case of nanomagnets, the oscillation and the relaxation times vary from less than one nanosecond to millions of years (Sellmyer and Skomski, 2006). Experimentally, it has been observed that the time dependence of the magnetization is often logarithmic rather than exponential (Sellmyer and Skomski, 2006) and the mathematical expression for the dynamics of magnetization process was first derived by Landau and Lifshitz in the form of non-linear differential equation (Stanescu, 2004). This equation was later on extended by Gilbert (1954) in which the effect of damping was included. The resulting equation of motion for the magnetization dynamics is known as Landau-Lifshitz-Gilbert (LLG) equation (Stanescu, 2004).

There are several reasons why research work in magnetization dynamics especially in different magnetic systems is at the heart of physics and the industrial world. One of such reasons is in the area of magnetic memories (Stanescu, 2004). One of the first magnetic

recording devices which was based on the magnetization dynamics used ferrite heads to write and read the information (Stanescu, 2004) and because the permeability in the ferrite falls above 10 MHz, the read or write process was possible only with a reduced rate but an important improvement was obtained using magnetic thin film. This was achieved by a thin magnetic film with permeabilities for applied frequencies larger than 300 MHz (Stanescu, 2004). Secondly, research in magnetization dynamics especially in thin magnetic layers with perpendicular anisotropy is of great importance in spintronics applications (Malinowski et al., 2009).

2.2 THEORETICAL BACKGROUND OF FERROMAGNETIC RESONANCE.

Resonance occurs when the energy levels of a quantized system of electronic or nuclear moments are Zeeman split by a uniform magnetic field and the system absorbs energy from an oscillating magnetic field at sharply defined frequencies which corresponds to transitions between the levels (Coey, 2010). Classically, resonance occurs when a transverse AC field is applied at the Larmor frequency (

the same principle. For EPR, the field,

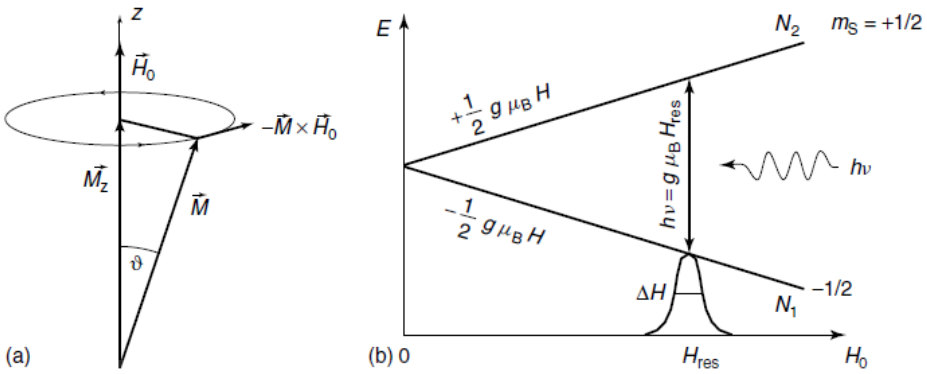

Figure 2.1: (a) is a sketch of the uniform precession of the vector

where

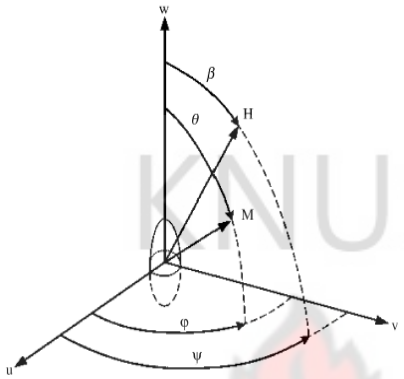

where ΔH_o is referred to as the inhomogeneous contribution to the linewidth. The inhomogeneous contribution of the linewidth in thin film is as a result of disorder. Firstly, the existence of fluctuations in the magnetic properties of the materials, such as its anisotropy or the magnetization leads to a linewidth that is frequency independent. Secondly, in FMR experiments, uniform precessional mode

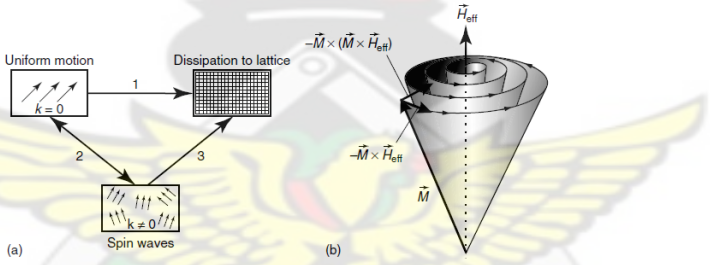

When the above matrix is simplified, this yields the famous Kittel equation for resonance frequency:

where

2.3 MAGNETIZATION IN ULTRATHIN MAGNETIC FILMS

Intrinsic magnetic properties such as magnetization, Curie point, anisotropy and magnetostriction in thin magnetic films may differ from their bulk counterparts. These differences result from the special environment that is provided by the surface and the interface atoms and also as a result of the strain which is induced by the substrate (Coey, 2010). In the case of ultrathin magnetic films, the ultrathin layer loses its internal degree of freedom. The exchange coupling in the thin ferromagnetic layer that are excited by the rf magnetic field that is uniform in the film plane keeps the magnetic moments across the film nearly parallel and hence the concept of giant magnetic moment can be applied to the individual layers (Mosendz, 2008). In the ultrathin film limit (thickness of the film < exchange length), the film behaves as an entity, as a giant magnetic molecule (Poulopoulos and Baberschke, 1999). The exchange length,

2.3.1 MAGNETIC ANISOTROPIES IN THIN FILMS

Ferromagnetic materials usually have two main axes namely; the easy and the hard axes. The amount of energy which is required to rotate the magnetization direction from the easy into the hard direction is referred as the magnetic anisotropy energy (Stöhr and Siegmann, 2006). Technologically, the magnetic anisotropy is one of the important properties of the magnetic materials. This is because depending on the type of application that a material is to be used, decision is made whether to use a high, medium or low magnetic anisotropy. Typical example is the perpendicular magnetic anisotropy (PMA) which is used for information storage and retrieval application (Johnson et al., 1996).

The spin orbit Hamiltonian (H) determines an important relationship between the magnetic anisotropy energy (MAE) and the orbital angular momentum. This relation is expressed as

where

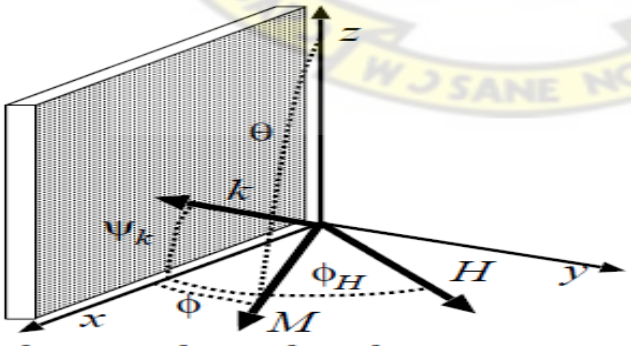

Figure 2.4: The coordinate system used to describe the orientation of the magnetization M, H and k with respect to the film (McMichael et al., 1998)

2.3.1.1 SHAPE ANISOTROPY

Shape anisotropy usually arises from the anisotropy of the demagnetization field, (

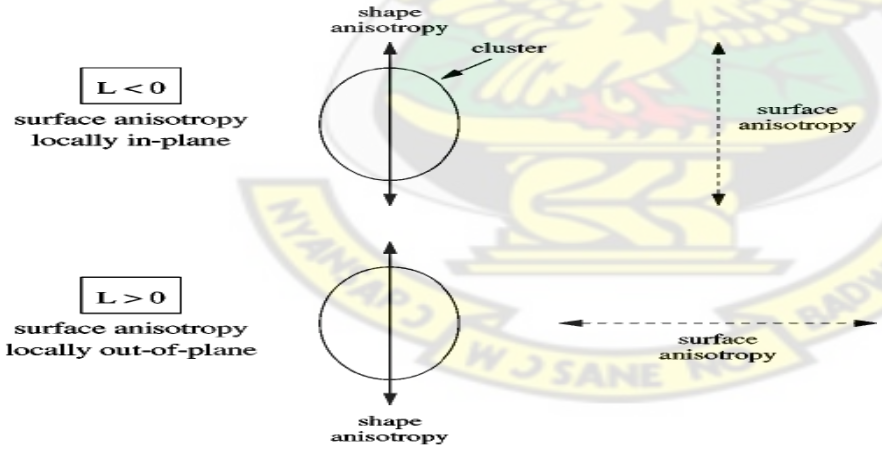
shape
anisotropy
cluster
L < 0
surface anisotropy
locally in-plane
surface
anisotropy
L > 0
surface anisotropy
locally out-of-plane
surface
anisotropy
shape
anisotropy

Thus shape and surface anisotropies gives opposite contributions and may even cancel each other in some particular system (Jamet et al., 2004)

2.3.1.2 MAGNETOCRYSTALLINE ANISOTROPY

The search for an understanding of the origin of magnetocrystalline anisotropy started many years before 1960 (Wang et al., 1993) and according to Van Vleck, the main origin of the magnetocrystalline anisotropy is as a result of the relativistic spin-orbit interaction of the electrons (Jamet et al., 2004) and the crystal field interaction (Coey, 2010). In the spin-orbit interaction, the electron orbitals are closely linked to the crystallographic structure and due to the interaction with the spins, they make the latter prefer to align along well-defined crystallographic axes (Getzlaff, 2008). This means that there are certain directions in space in which the magnetic material is easier to magnetize than the other and these are referred to as the easy and hard axes respectively (Getzlaff, 2008) . In addition to the crystal field interaction and the relativistic spin-orbit interaction, the exchange interaction and the dipolar interaction can also contribute to the magnetocrystalline anisotropy (Johnson et al., 1996). The difference between the exchange interaction and the dipolar interaction is that, the exchange interaction is independent of the angle between the spins and the crystal axes the dipolar interaction depends on the orientation of the magnetization relative to the crystal axes (Johnson et al., 1996).

Currently, an understanding of the magnetocrystalline anisotropy can be obtained from the ab initio bandstructure calculations and a typical example of such a calculation was carried out by Daaldrop in 1991, where he concluded that the symmetry of the state determines whether or not the state is split if the direction of the magnetization process is perpendicular or parallel to the film plane (Johnson et al., 1996). In magnetocrystalline anisotropy, the magnetization process is different when the magnetic field is applied along different crystallographic directions and this anisotropy reflects the crystal symmetry of the particular crystal system which is under consideration (Coey, 2010). Knowledge from magnetocrystalline anisotropy gives some insights

into which direction of the crystal has easy or hard magnetization direction and this can be helpful in the designing of new materials for information storage (Eriksson and Wills, 1999). Since the magnetic anisotropy energy (MAE) can be defined as the amount of work which is needed to rotate the magnetization from the easy to the hard directions, it means that if the rotation is carried out at constant temperature , then the magnetocrystalline anisotropy energy can also be defined as the change in the free energy F. When we consider a closed system, which is a system in which there is no exchange of particles between the system and its environment, it means that

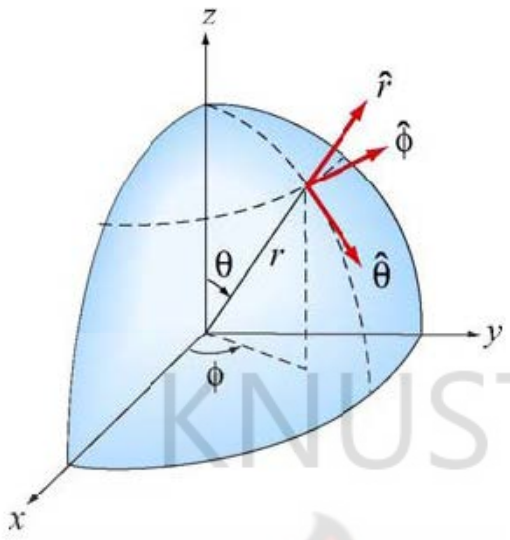

Figure 2.6: Spherical coordinates which is used in calculating the directional cosines.

The magnetocrystalline energy per volume (

Table 2.1: Shows the energy density, the crystallographic directions, the polar angles and the directional cosine for a cubic crystal (Getzlaff , 2008)

Energy density	Direction			Directional cosine
	[100]	90	0	
	[110]	90	45	
	[111]	54.7	45	

2.3.1.3 MAGNETIC SURFACES AND INTERFACE ANISOTROPIES

Magnetic surface and interface anisotropies are one of the most important magnetic anisotropies (Getzlaff, 2008) . Research interest in the area of magnetic properties of surfaces took centre stage in the early part of the 1970s (Kamzin et al., 1998). This intense interest was motivated by the need to understand the influence of ‘’defect’’ such as a surface on the formation of the properties of a surface layer and also on the processes which occur especially in the surface layer in the presence of the fundamental phenomena in the volume of the crystal (Kamzin et al., 1998). Also, interest in the magnetic properties of the surfaces and interfaces is as a result of its applications in devices especially the ultrathin magnetic films (Rickart et. al, 2004) and the deep connection between the magnetic surfaces and interface to the magnetic oligatomic films and artificial superstructures (Gradmann, 1986). One of the excellent tools which is used for the experimental analysis of magnetic surface anisotropies is the torsion oscillation magnetometry (TOM) which provides quantitative data on the magnetic surface and out-of-plane anisotropy of an ultrathin films with monolayer resolution (Gijs and Petroff, 1997) .

The concepts of magnetic surface anisotropy (MSA) was predicted theoretically by Néel (1954) (Elmers and Gradmann, 1994) and this magnetic anisotropies result from the broken local symmetry as a result of the contribution to the surface energy which depends on the orientation of the magnetization on the surface (Bruno and Seiden, 1988). Néel proposed that the surface energy,

out of plane MSA. Gradmann et.al later proposed the need for an additional term to this surface energy which takes into account the use of the polar coordinates

2.4 LINEWIDTH AND LINESHAPE

Spin resonance lines in solids are broadened by a number of mechanisms. Some of these mechanisms give rise to a Gaussian lineshape, strain broadening and the Lorentzian lineshape (Stoneham, 1972). The Gaussian lineshape occurs as a result of the dipolar broadening in concentrated crystals and strain broadening results from dislocation in the crystal system (Stoneham, 1972). In the case of the Lorentzian lineshape, broadening occurs due to the finite lifetime of a state (Stoneham, 1972).

In spin resonance, what is commonly observed is the derivative of the lineshape rather than the shape itself (Stoneham, 1972). The analysis of the peak-to-peak separation,

is the Gaussian lineshape (Brown, 1991). The Gaussian and the Lorentzian lineshapes are represented by equations (2.27) and (2.28) respectively as (Petrakis, 2000) :

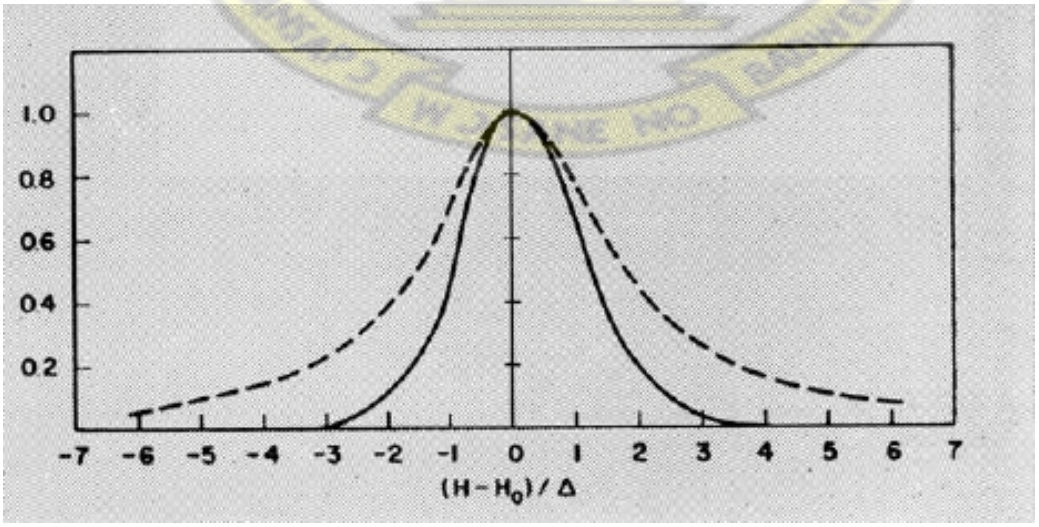

Figure 2.7: Zero derivative curve for Gaussian (solid line) and Lorentzian (broken) shape function (Leonides Petrakis, 2000)

If each of the expressions in (2.27) and (2.28) is differentiated twice, set to zero and solved for

CHAPTER THREE

3 METHODOLOGY

3.1 INTRODUCTION

In this section of the thesis, the experimental methods adopted in this work are discussed. These include; sample preparation and the Bruker ElexSys E500 EPR spectrometer and the experimental procedure.

3.1.1 SAMPLE PREPARATION AND THE BRUKER ELEXSYS E500 EPR SPECTROMETER

$La_{0.7}Sr_{0.3}MnO_3$ (LSMO) thin film of different unit cells thicknesses were fabricated using the pulsed laser deposition (PLD) technique (KrF excimer, λ=248 nm) with a pulse energy density of 1-2J/cm^3 on (001)

The energy which is dissipated per cycle in eqn. (3.1) is the amount of energy which is lost during the microwave period. In the cavity also, some amount of energy can be lost to the side walls as a result of the fact that the microwaves generate electrical currents in the side walls which in turn generate heat (Jiang and Weber, 2001).

Ferromagnetic resonance (FMR) measurements were carried out with a Bruker ElexSys E500 EPR spectrometer using an X-band frequency of 9.75 GHz microwave source and a

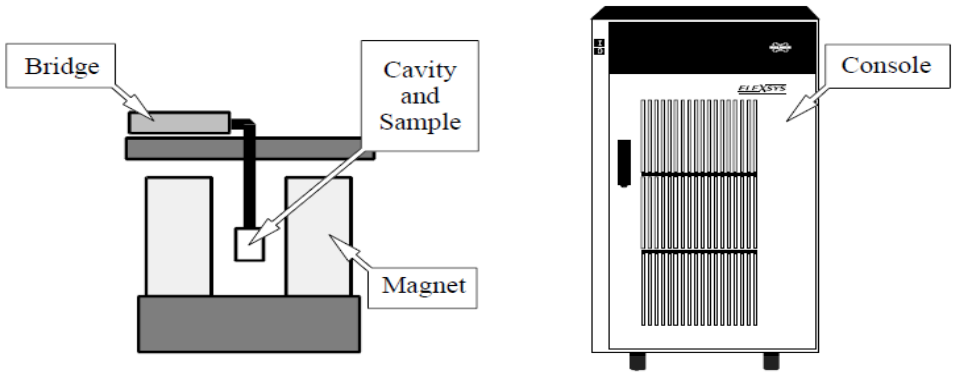

Figure 3.1: The general outline of an EPR spectrometer (Jiang and Weber, 2001)

In fig 3.2, A is the microwave source whose output power cannot easily be varied. After the microwave source, A, is point B, a variable attenuator which blocks the flow of the microwave radiation. The microwave power which the sample sees can precisely and accurately be controlled with the attenuator. The circulator at point C, allows microwave radiation coming back from the cavity to be detected by the detector. In the circulator, microwaves coming in port 1 only go through port 2 and not directly to the detector through port 3. Point E, in fig 3.2 is a Schottky barrier which detects the reflected microwave and also converts the microwave power to an electrical current. Point F is a reference arm whose function is to supply the detector with some extra microwave power or ‘’bias’’. For Bruker ElexSys E500 electron paramagnetic resonance (EPR) spectrometer which operates at the X-band frequency of 9.75 GHz in the continuous wave (CW) mode two main resonators can be used. The first one is a super high sensitivity resonator with optical port which is suitable for most organic and inorganic samples. The second one is a dual-mode ER4116DM resonator, which allows the microwave to be applied either perpendicular or parallel to the sample axis and is specifically designed for anisotropic studies of triplets, biradicals of transition metal and rare earth ions containing "forbidden" fine structures or hyperfine structure transitions. But in the case of this thesis work, the ER4116DM

was used because of the anisotropic studies (magnetic property i.e. resonance position and full width half maximum), the low temperature behavior, angular dependence of the FMR signal of 15 uc LSMO thin film sample and ferromagnetic resonance in other LSMO thin films of varying unit cells which was of main concern.

Temperature control of the LSMO thin film sample can be done in three different ways and this depends on the temperature regime which is of interest and the availability of that temperature control system. A variable temperature system using liquid nitrogen boil-off air is regularly set up for temperatures ranging from room temperature (300 K) down to about 100 K. A finger Dewar can be used for measurement at 77 K and a liquid helium cryostat system can be used for meaurement at 4 K. In this study, the liquid nitrogen was used because we were interested in carrying out the magnetic property, the low temperature behavior and the angular dependence of the 15 uc LSMO thin film at 150 K, 200 K and 250 K.

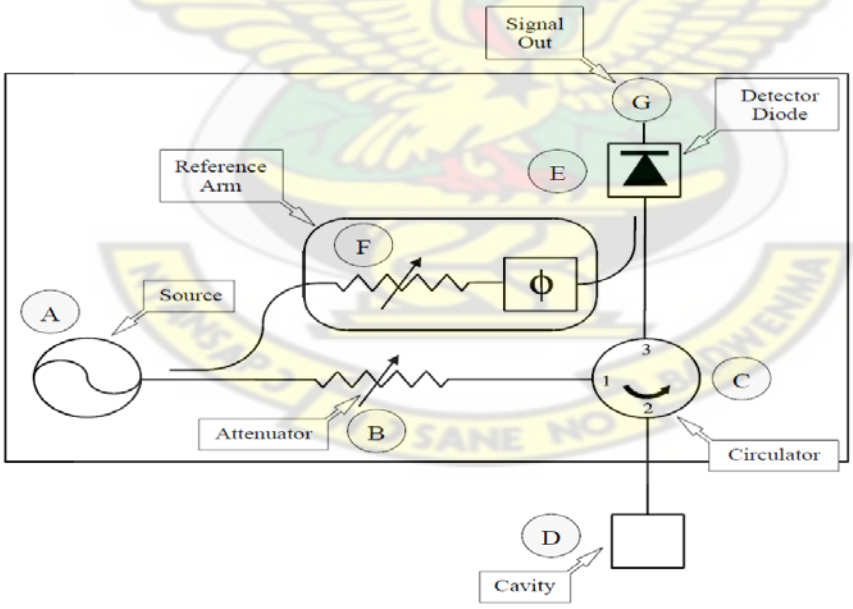

Figure 3.2: Block diagram of a microwave bridge.(Jiang and Weber, 2001)

3.1.2 EXPERIMENTAL PROCEDURE

Ferromagnetic resonance (FMR) measurement was carried out on the 15 unit cell (uc) thick $La_{0.7}Sr_{0.3}MnO_3$ (LSMO) thin film. This was done by positioning the 15 unit cell (uc) thick LSMO thin film in a particular orientation [110] in the quartz sample holder made of glass. The quartz sample holder which contains the LSMO thin film was inserted into the microwave cavity of the ElexSys E500 spectrometer for angular dependence of FMR spectrum to be recorded on the computer. This was achieved by rotating the sample holder which contains the LSMO thin film with a goniometer which was mounted on top of the microwave cavity of the Bruker ElexSys E500 spectrometer. The electromagnet was used in supplying magnetic field to the LSMO thin film. The applied dc magnetic field was swept through the LSMO sample in the microwave cavity till resonance was achieved. At resonance, the power which is absorbed by the LSMO thin film is a maximum. The FMR spectrum which was observed at a frequency of 9.75 GHz, with a power of 0.6325 mW, tolerance of 1.00 K, modulation frequency of 100.00 kHz, modulation amplitude of 10.00 and power attenuation of 25.0dB was recorded on the personal computer. In order to avoid contaminating the microwave cavity of the Bruker ElexSys E500 spectrometer with paramagnetic contaminants which produces spurious EPR signals, the quartz sample holder was consistently wiped with a tissue paper.

Angular dependence of FMR spectra were recorded with the magnetic field rotated in the film plane (in-plane geometry i.e. magnetic field is applied parallel to the thin film) or in the plane which is perpendicular to film plane (i.e. out -of-plane geometry). It should be noted that due to restrictions of the experimental setup in the in-plane geometry, the microwave magnetic field is perpendicular to the film while in the case of the out-of-plane geometry, the resonance field is in the plane of the film. The coordinate system which was used for the measurement and

analysis of the out-of-plane dependence is as shown in fig 3.3. In the ferromagnetic resonance (FMR) measurement of the 15 uc thick LSMO thin film at 150 K, the out-of-plane orientation was carried out by a goniometer which was fixed to the spectrometer. The goniometer rotates in steps of 1^0. Generally, in FMR the angle,

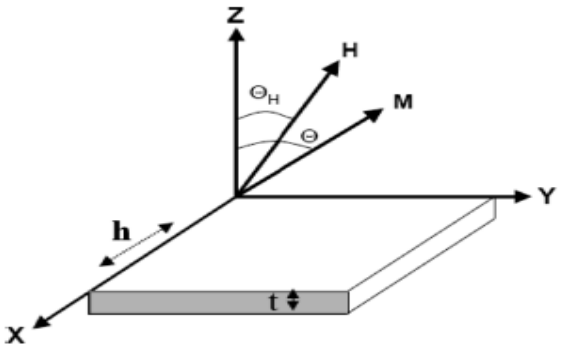

Figure 3.3: Coordinate system used for the measurement and analysis of the out-of-plane angular dependence of FMR (Yilgin et al., 2005)

CHAPTER FOUR

4 RESULTS AND DISCUSSIONS

The recorded signal versus the field for the 15 uc LSMO thin film sample at 200 K and 250 K is as shown in fig 4.1 and fig 4.2. As it can be observed in fig 4.1 and fig 4.2, the base line is at the zero-mark and this quiet significant. Fig 4.1.and fig 4.2 shows that FMR phenomenon occurred in the 15 uc LSMO thin film at 200 K and 250 K. Fig 4.3 shows the variation of the in-plane angular dependence of the resonance field. This in-plane angular dependence of the resonance field (FMR spectrum) was observed for the 15 uc thick LSMO thin film sample at 150 K. According to Kwon et al., 2011 the presence of in–plane ferromagnetic resonance in LSMO can be attributed to the distribution of anisotropies in the thin film. Also, this in-plane angular dependence of the resonance field might be attributed to unidirectional and uniaxial anisotropies in the LSMO thin film. As shown in fig 4.3, the resonance spectrum evolves as the field is rotated in the in-plane orientation (i.e. magnetic field is applied parallel to the thin film). Clearly, the resonance spectrum is sinusoidal-like in nature and this is consistent with earlier research work which was conducted on LSMO bicrystalline thin film sample at 150 K and 9.5 GHz on STO substrate (Alejandro et al., 2010). It can be seen in fig 4.3, that there is a critical orientation where only uniform FMR mode can be observed. According to Puszkarski (1970) the presence of the single uniform FMR mode is due to surface anisotropy field at the surface of a ferromagnetic film such as LSMO which allows excitation of an exchange-dominated non-propagating surface mode (Liu et al., 2007). The main feature of the FMR spectrum of the 15 uc LSMO thin film is a single FMR line and this is consistent with Alejandro et al., 2010 in which ferromagnetic resonance experiment was conducted on (La,Sr)MnO_3 bicrystalline films at 150 K on STO substrate.

In the research work conducted, it was observed in fig 4.3 that the maximum orientation resonance fields occurred at 15^0, 46^0, 104^0 and 151^0 whiles the minimum orientation resonance fields occurred at 28^0, 77^0, 118^0 and 167^0. In order to confirm the nature of our plot in fig 4.3, xmgrace software was also used in plotting the sets of data from our experiment and the result were almost the same as the one which were generated using the Matlab. Xmgrace software was also used in confirming the nature of our plots in fig 4.6 and fig 4.7 to the plots which were generated in Matlab. The mean maximum and mean minimum of the resonance fields of the 15 uc thick LSMO thin film sample were 1229.5 Oe and 910.875 Oe respectively. The resonance position of our plot in fig 4.3 is the average of the sum of the mean minimum and mean of maximum resonance fields while the width of the resonance spectrum (FWHM) is the mean of the difference between the maximum and minimum resonance fields. The resonance position of the 15 uc LSMO thin film sample from our plot was 1070.1875 Oe and the resonance width (FWHM) was 159.3125 Oe respectively. The resonance position in fig 4.3 might be as a result of the in-plane anisotropy and the resonance width might be attributed to disorder in the LSMO thin film (Beaujour et. al, 2006). This disorder is as a result of two main factors. Firstly, fluctuations in magnetic properties of the material such as magnetization and secondly as a result of the fact that in a typical ferromagnetic resonance experiment, uniform precessional mode (

result of film substrate (STO) thermal expansion mismatch, lattice mismatch or the film microstructure (Srivastava et al., 1999).

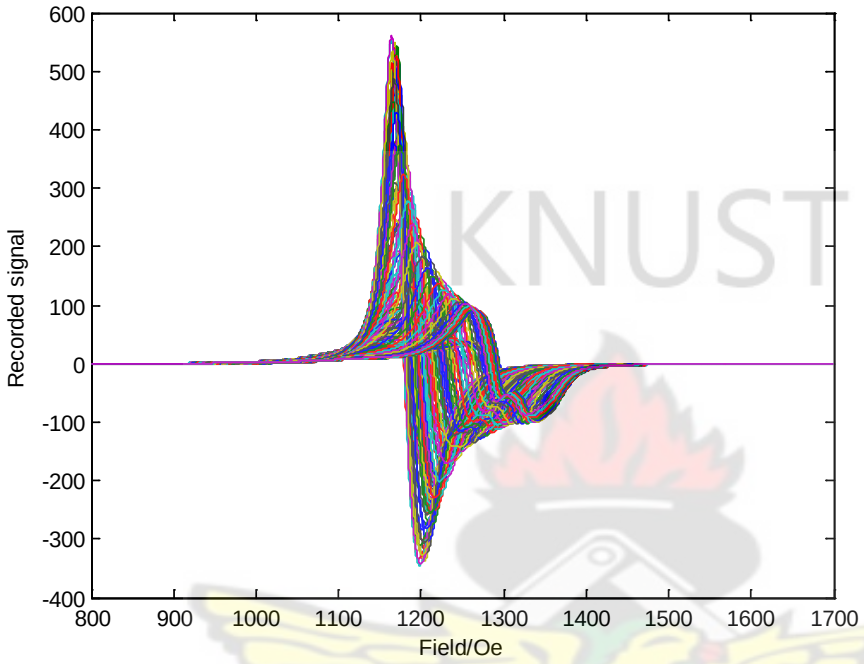

Figure 4.1: Recorded signal versus field /Oe (FMR spectra) for the 15 uc LSMO thin film sample at 200 K and 9.75 GHz.

Research by Baselgia et al., 1988 has shown that sometimes there are discrepancies in the angular dependence of the FMR spectrum especially in the perpendicular (out-of-plane) or in the plane configuration of the external field. These discrepancies might have affected our results because in most studies of FMR, the Smit and Beljers model are used. The discrepancy according to Baselgia et. al, 1988 can be attributed to the fact that the free energy density (F), contains different terms which result in angular mixing which cannot be eliminated in the Smit and Beljers model for the resonance equation. This discrepancy can be eliminated by using the modified form of the Smit and Beljers model (Baselgia et al., 1988).

The resonance field versus the angle for both simple position and simple width for various unit cells (uc) of the LSMO thin film at 150 K is as shown in fig 4.6 and fig 4.7 respectively. It can be observed from fig 4.6 and fig 4.7 that in all different unit cells of the LSMO thin films, the resonance field seems to have a minimum from 0^0 to 100^0 and the resonance field seems to have a maximum within a swept angle of 100^0 to about 150^0.

In fig 4.5, the temperature dependence of the FMR spectra of the 15 uc LSMO thin film at different temperatures was observed from the plot of the recorded signal versus field. These temperatures were 150 K, 200 K and 250 K. It can be observed from the plot of the recorded signal versus the field (FMR spectra) that as the temperature increases, the ferromagnetic resonance spectra shifts to higher fields and this might be as a result of the transition into ferromagnetic state. This is consistent with Tovstolytkin et al., 2004 when FMR measurements were performed on LSMO thin film in the temperature range of 77 K to 300 K using a RADIOPAN spectrometer which operates at 9.2 GHz.

Fig 4.10, fig 4.11 and fig 4.12, shows the plots of the recorded signal versus the angle(angular dependence of the FMR signal). Clearly, the plots of the angular dependence of the FMR signal is a complicated phenomena and this might be as a result of shape effects in the LSMO thin film (Pradhan et al., 2006). The variation could also arise from other contributions such as different residual stress in the films as discussed in other reports. Apart from the above mentioned factors which might have caused such a complicated phenomena in the 15 uc LSMO thin film, thermal expansion coefficient mismatch between the substrate (STO) and the thin film (LSMO) might have also contributed to it. Generally, when LSMO thin film is fabricated on STO substrate, due to thermal expansion coefficient mismatch; this generates a crystal misfit which is less than 1% for all temperatures below 1000 K. Fig 4.13 and fig 4.14 also shows the

angular dependence of the FMR signal at various temperatures (150 K, 200 K and 250 K). These figures indeed also confirm to the fact that the angular dependence of the FMR signal at various temperatures is a complicated phenomena. Fig 4.8 and fig 4.9 shows the surface plots for the signal, field and angle which confirms FMR phenomenon in LSMO thin film.

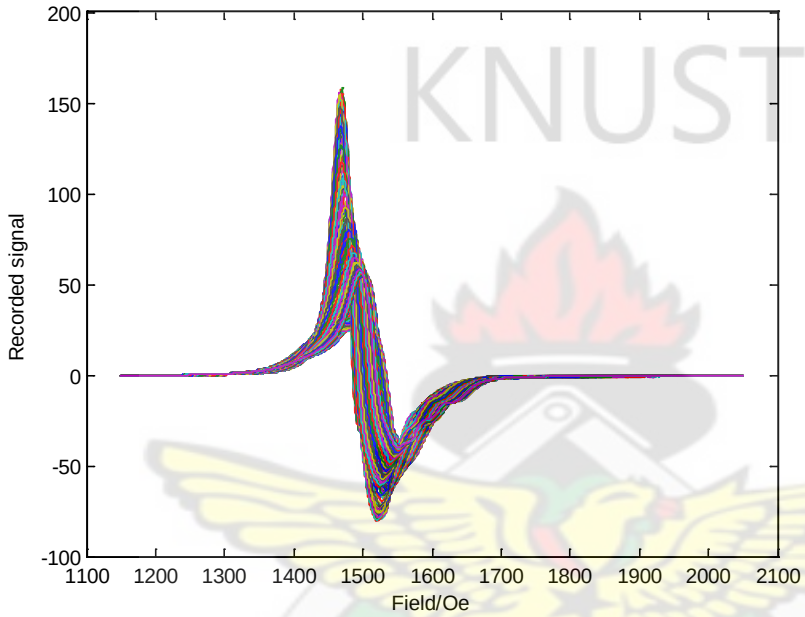

Figure 4.2: Recorded signal versus field /Oe (FMR spectra) for the 15 uc LSMO thin film sample at 250 K and 9.75 GHz.

In-plane angle /^{0}

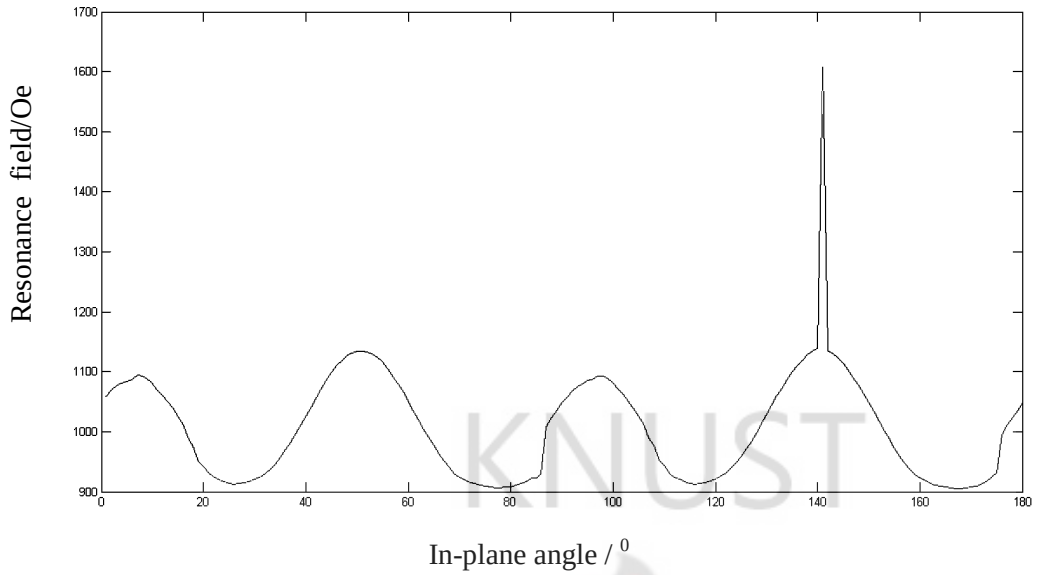

Figure 4.3: Resonance field /Oe versus in-plane angle/^{0} of the 15 uc LSMO thin film sample at 150 K and 9.75 GHz.

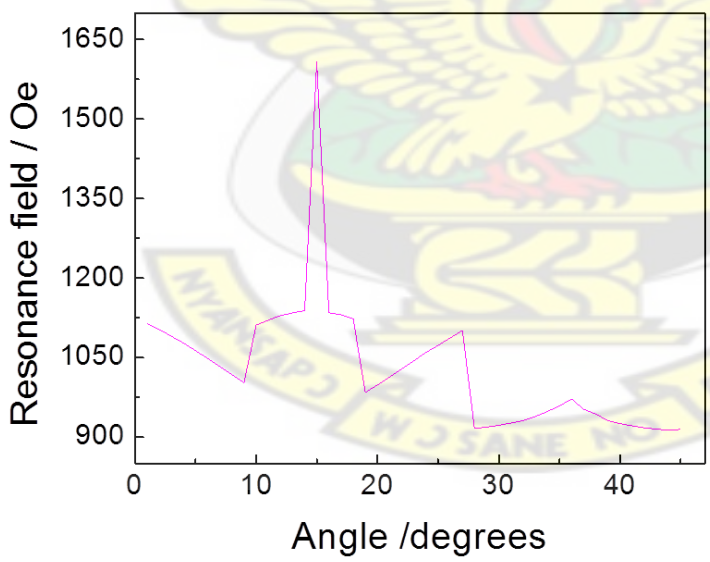

Figure 4.4: Resonance field/ Oe versus angle/^{0} of the 15 uc LSMO thin film sample at 150 K and 9.75 GHz.

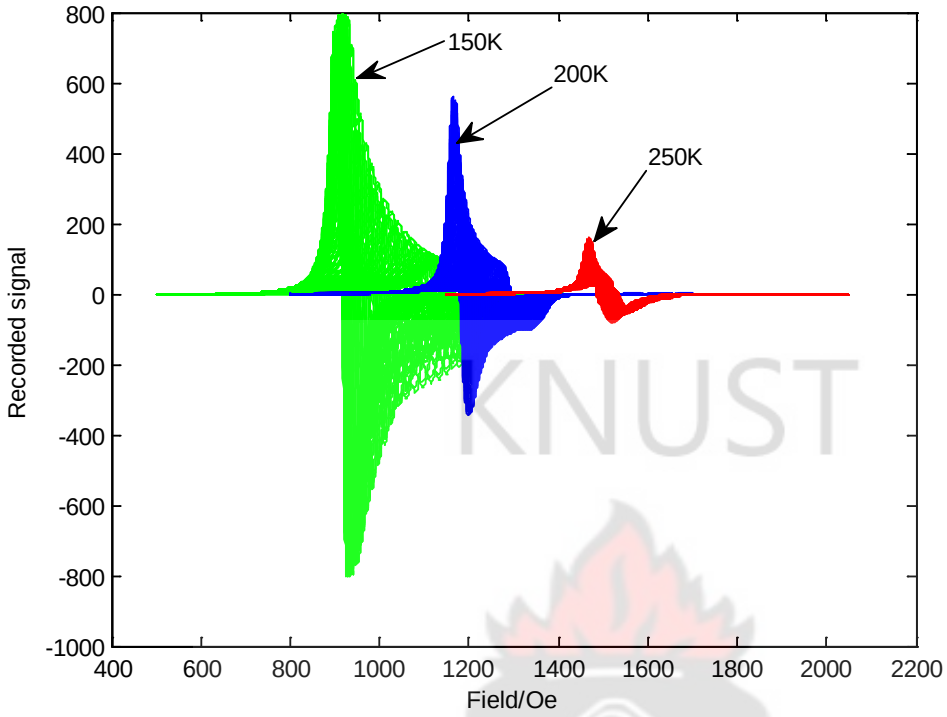

Figure 4.5:

Recorded signal versus field /Oe (FMR spectra) at different temperatures (150 K, 200 K and 250 K) and 9.75 GHz for the 15 uc LSMO thin film sample.

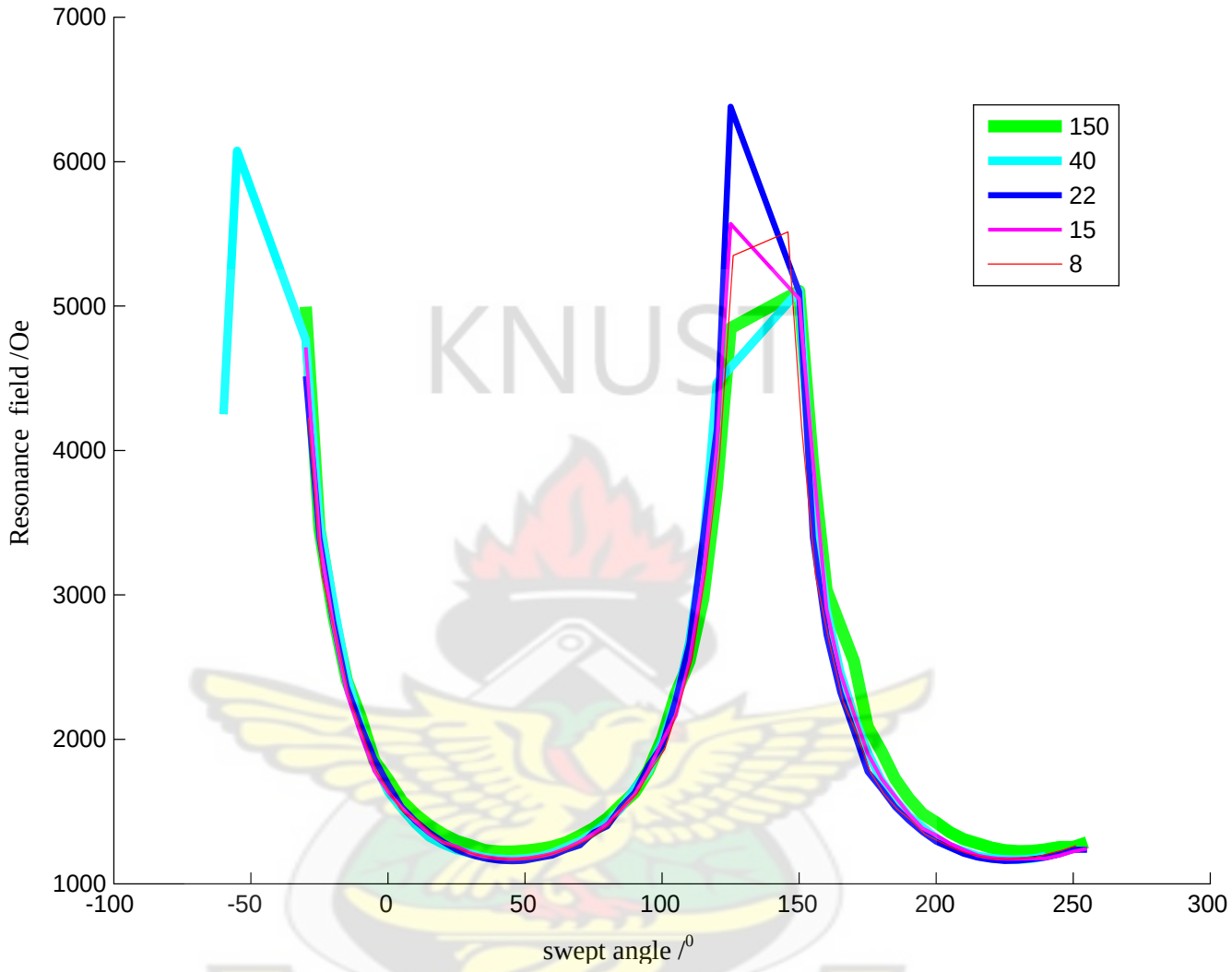

Figure 4.6: Resonance field / Oe versus swept angle/^{0} of simple position of various unit cell [uc] of LSMO thin film of varying thicknesses at 150 K.

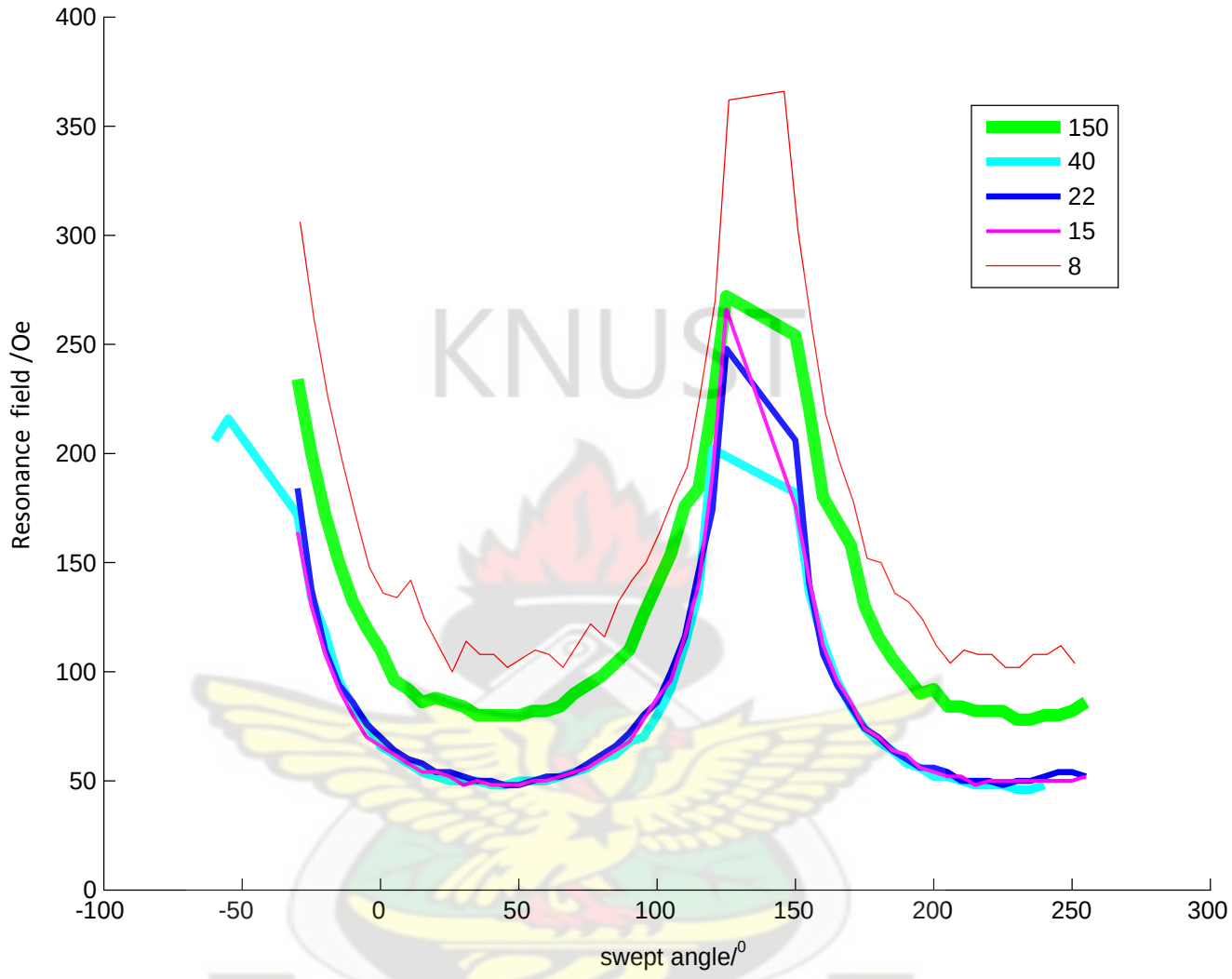

Figure 4.7: Resonance field/ Oe versus swept angle/ ^{0} of simple width of various unit cell [uc] of LSMO thin film of varying thicknesses at 150 K

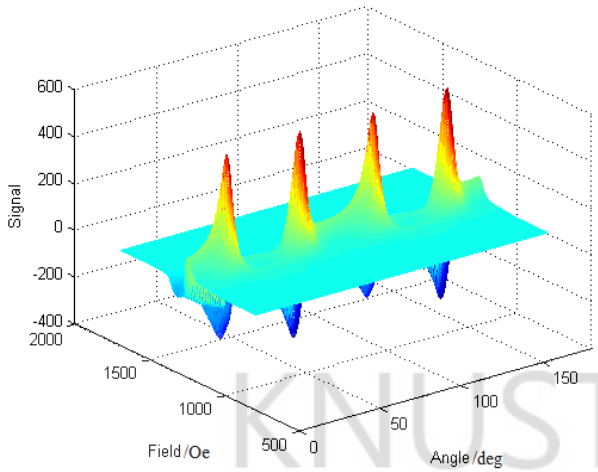

Figure 4.8: Surface plot of the 15 uc LSMO thin film at 200 K which confirms FMR in LSMO.

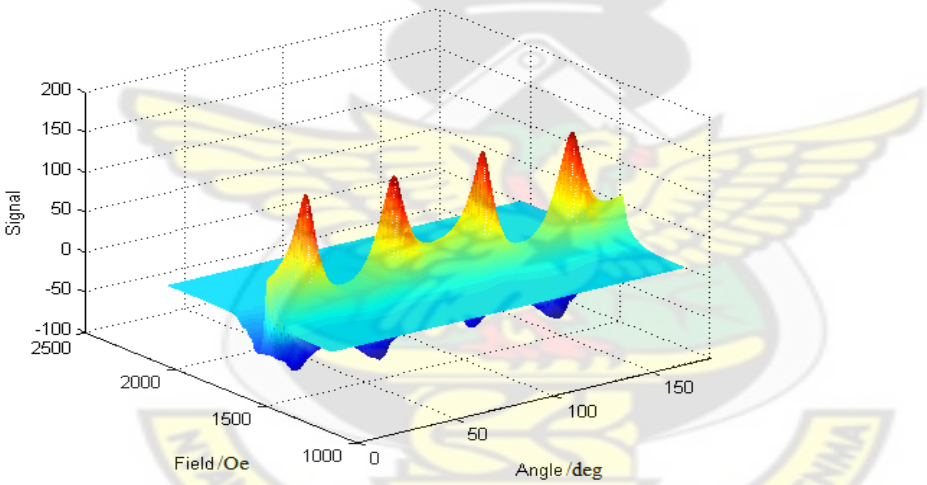

Figure 4.9: Surface plot of the 15 uc LSMO thin film at 250 K which confirms FMR in LSMO

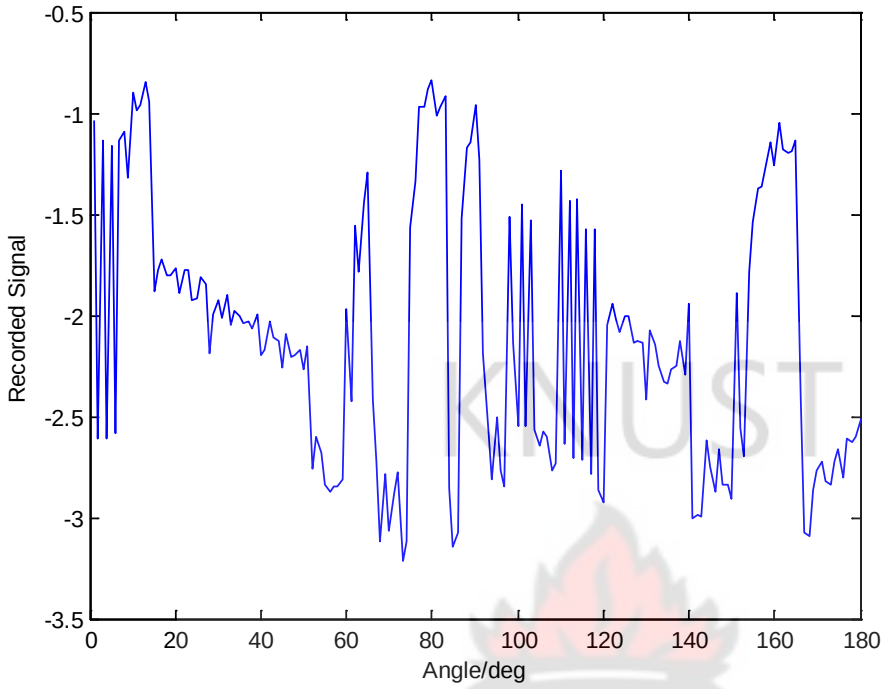

Figure 4.10: Recorded signal versus angle/^{0} of the 15 uc LSMO thin film at 150 K.

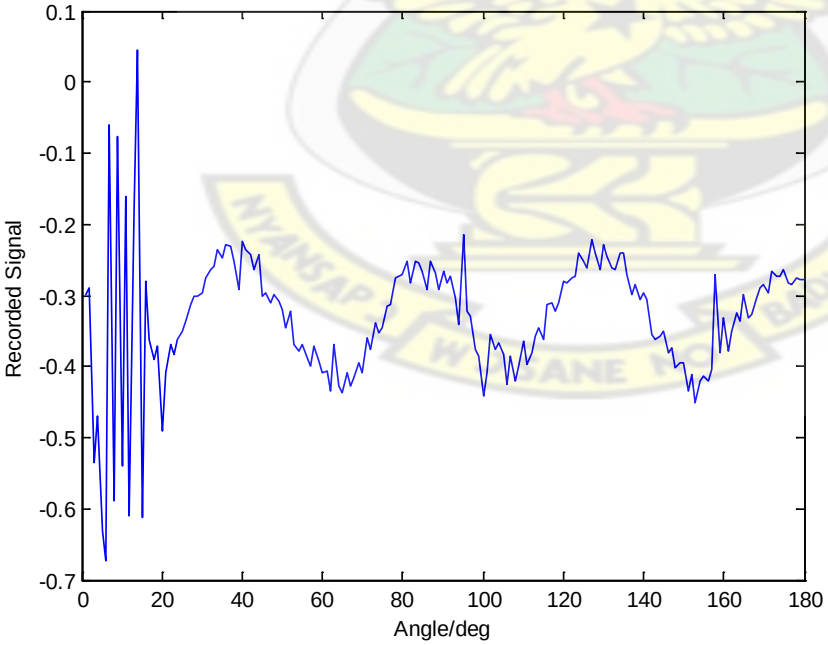

Figure 4.11: Recorded signal versus angle/^{0} of the 15 uc LSMO thin film at 200 K.

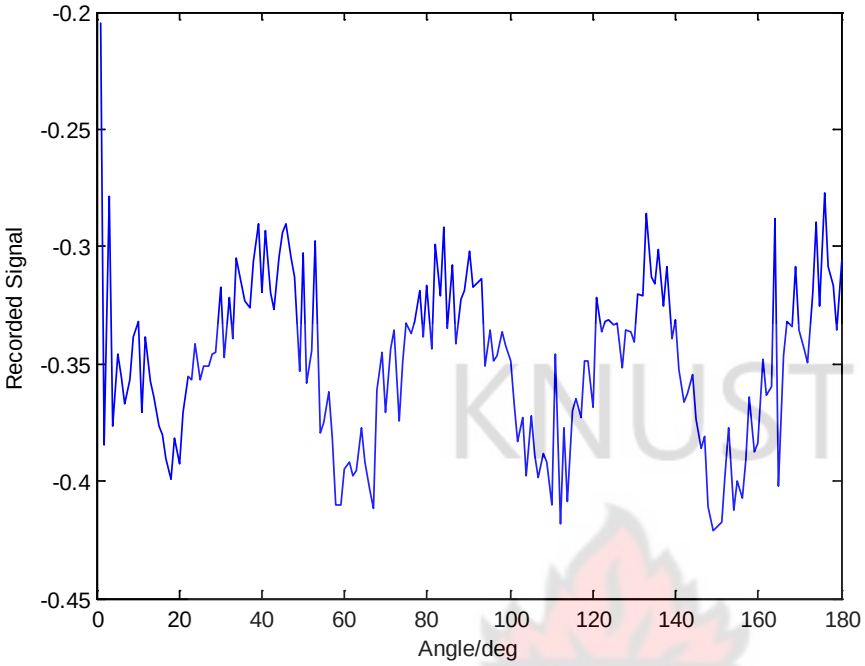

Figure 4.12: Recorded signal versus angle/deg of the 15 uc LSMO thin film at 250 K.

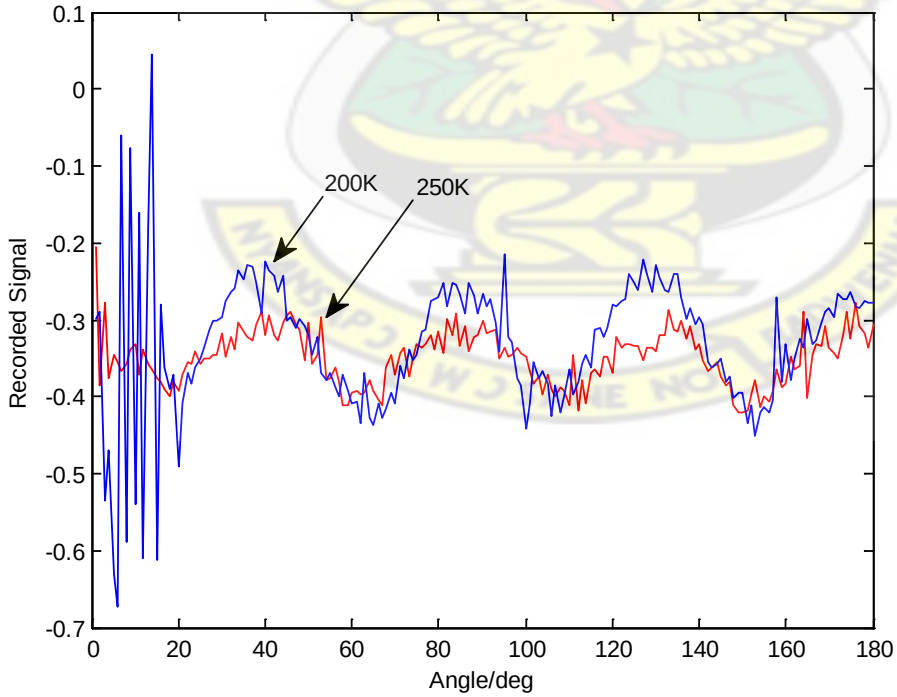

Figure 4.13: Recorded signal versus angle/deg of the 15 uc LSMO thin film at 200 K and 250 K.

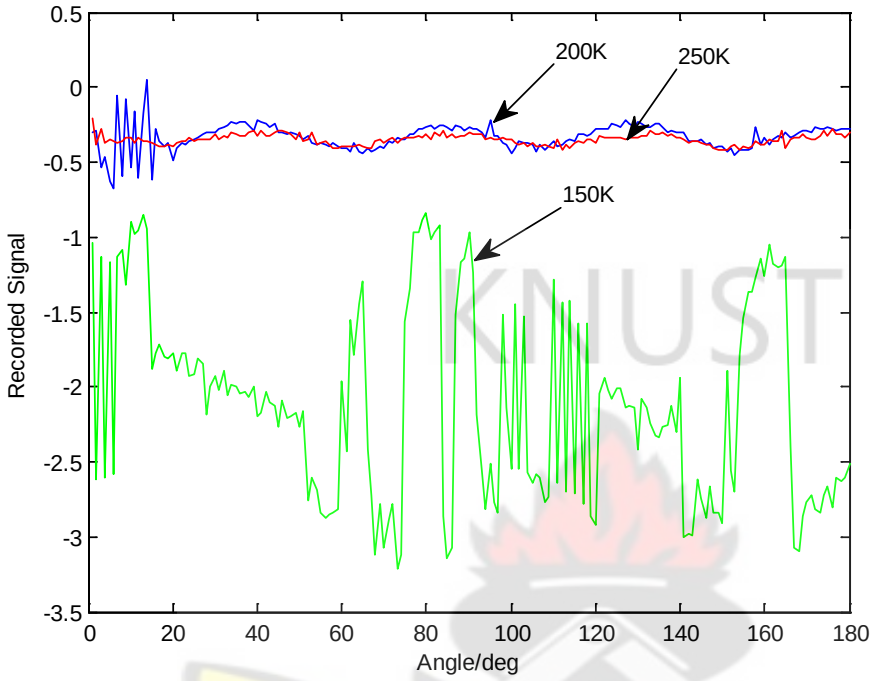

Figure 4.14: Recorded signal versus angle/deg of the 15 uc LSMO thin film at 150 K, 200 K and 250 K.

CHAPTER FIVE

5 CONCLUSIONS AND RECOMMENDATIONS

5.0 CONCLUSIONS

The magnetic property, the temperature dependence of the FMR spectra and the angular dependence of the FMR signal of the 15 uc LSMO thin film on STO substrate has been studied using FMR technique. FMR phenomena in other unit cells (uc) has also been established. The resonance position and the full width half maximum (FWHM) of the 15 uc LSMO thin film were 1070.1875 Oe and 159.3125 Oe respectively. The resonance field versus the in-plane angle was sinusoidal-like in nature as expected. The plot of the recorded signal versus the field at various temperatures (150 K, 200 K and 250 K) revealed that as the temperature increases, the ferromagnetic resonance (FMR) spectra shifts to higher fields. Finally, it has been established that the angular dependence of the FMR signal showed a complicated phenomenon.

5.1 RECOMMEDATIONS

- Since the investigation of ferromagnetic resonance is an experimental technique which can be used in determining the magnetic properties of thin films further research can also be done on the frequency dependence of the resonance field, H_{res} which determines the gyromagnetic ratio so that the g-factor can also calculated for the LSMO samples.
- Due to discrepancies between experimental results and theory for the frequency at which resonance occurs using the Smit and Beljers model, the modified model which was proposed by Baselgia et. al (1988), which avoids mixing in the free energy density, F which obscures the angular dependent terms can be used instead.
- Different fundamental magnetic properties or behavior such as magnetic anisotropy and domain structure of LSMO thin films grown on different substrates can be investigated.
- Study of different strain state on structural and magnetic properties of expitaxial LSMO films which can be grown on different substrates such as $SrTiO_3$ (STO) of (001) orientation and $NdGaO_3$(NGO) of (001) of different orientations (eg. (100), (010), (110) and (001)) can be investigated.
- X-ray diffractometer can be used for structural analysis of LSMO thin films which is fabricated on $SrTiO_3$(001). This can be used to ascertain or confirm the fact that LSMO thin film grows in two–dimensional growth mode resulting in an epitaxial film replicating the step-terrace of the substrate up to the film surface.
- Magnetic anisotropy measurements of LSMO film of different thicknesess at different temperatures can be carried out by both Vibrating sample magnetometer (VSM) and Torque magnetometry.

- Magnetization reversal mechanism of LSMO/NGO (100) thin film can be studied so that curling model and modified Kondorsky model can be compared.
- Magnetization(M) and magnetic hysteresis measurements can also be conducted using a superconducting quantum interference device (SQUID) magnetometer with in-plane magnetic field where the effect of annealing on the LSMO can be investigated. Thus magnetization and magnetic hysteresis measurements can be conducted before and after annealing to see if there is any change in these magnetic quantities
- Electrical transport studies can also be conducted using the four-probe ac technique.

6 REFERENCES

Alejandro G., Steren L.B., Pastoriza H., Vega D., Granada M., Sanchez Rojas J.C., Sirena M. and Alascio B. (2010). Magnetoresistance effect in (La,Sr)MnO_3 bicrystalline films. Journal of Condens. Matter, 22: 346007

Brivio S., Magen C., Sidorenko A.A., Petti D., Cantoni M., Ciccacci M., De Renzi R.,Varela M., Picozzi S. and Bertacco R. (2010). Effects of Au nanoparticles on the magnetic and transport properties of $La_{0.67}Sr_{0.33}MnO_3$ ultrathin layers. Physical Review B, 81: 094410

Baselgia L., Warden M. and Waldner F., Hutton Stuart L., Drumheller John E., He Y.Q. and Wigen P.E. (1988). Derivation of the resonance frequency from the free energy of ferromagnets. Physical Review B, 38(4)

Bruno P. and Seiden J. (1988). Theoretical investigation on magnetic surface anisotropy. Journal of Physics, 49 (12)

Bruno P. and Renard J. P. (1989). Magnetic surface anisotropy of transition metal ultrathin films. Appl. Phys. A, 49

Brown Ron (1991). All peaks aren't Gaussian. Physical Review B, 40(3).

Baberschke Klaus (2007). Investigation of Ultrathin Ferromagnetic Films by Magnetic Resonance. Handbook of Magnetism and Advanced Magnetic Materials. Volume 3

Bah R., Bitok D., Rakhimov R.R., Noginov M.M., Pradhan A.K. and Noginova N. (2006). Ferromagnetic resonance studies on colossal magnetoresistance films: Effects of homogeneity and light illumination. Journal of Applied Physics, 99: 08Q312

Beaujour J.M, Ravelosona D., Tudosa I., Fullerton E. and Kent A.D. (2009). Ferromagnetic resonance linewidth in ultrathin films with perpendicular magnetic anisotropy. Phys. Rev. B, 80: 180415 (R).

Celinski Z., Urquhart K.B. and Heinrich B. (1997). Using ferromagnetic resonance to measure the magnetic moments of ultrathin films. Journal of Magnetism and Magnetic Materials 166

Chikamatsu A., Wadati H., Kumigashira H., Oshima M., Fujimori A., Hamada N., Ohnisha T., Lippmaa M., Ono K., Kawasaki K. and Koinuma H. (2008). The band structure and Fermi surface of $La_{0.6}Sr_{0.4}MnO_3$ thin films studied by in-situ angle-resolved photoemission spectroscopy. Physical Review B, 56

Coey J.M.D. (2010). Magnetism and Magnetic Materials. Cambridge University Press, New York,

Coey J.M.D., Viret M. and Ranno L. and Ounadjela K. (1995). Electron Localization in Mixed- Valence Manganites. Physical Review Letters, 75 (21) :3910-3913.

Coey J.M.D, Viret M. and Molnar S.Von (1999). Mixed –valence manganites. Advances in Physics, 48(2): 167-293.

Covington M., Crawford T.M. and Parker G.J.(2002). Time-resolved measurement of propagating spin waves in ferromagnetic thin films. Physical Review Letters, 89 (23): 237202.

De Jong M.P., Bergenti I., Dediu V.A., Fahlman M., Marsi M. and Taliani C. (2005). Evidence for Mn^{2+} ions at the surface of $La_{0.7}Sr_{0.3}MnO_3$ thin films. Physical Review B, 71: 014434

Duan Chun-Gang, Velev Julian P., Sabirianov R.F., Mei W.N., Jaswal Sitaram and Tsymbal Evgeny Y. (2008). Tailoring magnetic anisotropy at the ferromagnetic / ferroelectric interface. Applied Physics Letters, 92

Dubowik J. and Gos´cian´ska I. (2008). Ferromagnetic resonance in metallic thin film and thin film tubes. Acta Physica Polonica A, 113 (1): 179-182.

Elmers H.J. and Gradmann U. (1994). Dependence of magnetic surface anisotropies on symmetries of a nonmagnetic overlayer. Surface Science 304.

Eriksson O. and Wills J. (1999). First Principles Theory of Magnetocrystalline Anisotropy. Springer.

Farag N., Bobeth M., Pompe W., Romanov A.E. and Speck J.S. (2005). Rhombohedral LSMO films- a unique case of ferroelectricity domain formation. Phys. Stat. Sol. (a)202 (4):R44-R46

Farle Michael (1998). Ferromagnetic resonance of ultrathin metallic layers. Rep. Prog. Phys. 61: 755-826.

Gomez J. and Butera A. (2004). Ferromagnetic resonance linewidth in $Co(x)-SiO_2(1-x)$ granular films. Physica B, 354: 145-148

Gor´kov Lev P. and Kresin Vladmir Z. (2004). Mixed-Valence Manganites: fundamentals and main properties, Physics Report 400: 149-208.

Gommes I.T., Almeida B.G., Lopes A.M.L., Araujo J.P., Barbosa J., Mendes J.A. (2010). Structural and magnetic characterization of $LaSrMnO_3$ thin films deposited by laser ablation on MgO substrate. Journal of Magnetism and Magnetic Materials, 322: 1174-1177

Getzlaff Mathias (2008). Fundamentals of Magnetism. Advanced Magnetic Nanostructures. Springer Science and Business Media Inc ; New York pp 80-82

Gradmann Ulrich (1986). Magnetic surface anisotropies. Journal of Magnetism and Magnetic Material: 54-57

Gijbs M.A.M and Petroff F. (1997). Magnetic Ultra Thin Films, Multilayers and Surfaces. Elsevier Science BV

Gradmann U. and Elmers H.J. (1999). Magnetic surface anisotropies in NiFe-alloy films: Separation of intrinsic Néel type from strain relaxation contributions. Journal of Magnetism and Magnetic Materials 206

Grivet J.P. (1997). Accurate numerical approximation to the Gauss-Lorentz lineshape. Journal of Magnetic Resonance, 125

Golosovsky M., Monod P., Muduli P.K. and Budhani R.C. (2007). Spin-wave resonances in $La_{0.7}Sr_{0.3}MnO_3$ films: Measurement of spin-waves stiffness and anisotropy field. Physical Review B, 76: 184413

Hartwell John. W. (1968). Standing spin waves in ferromagnetic thin films. Proceedings of the IEEE, 56 (1): 23-31.

Harada I. and Nagai O. (1979). Spin – waves excitations in ferromagnetic thin films with nearest-neighbor and next- nearest-neighbor exchange interactions. Physical Review B, 19 (7): 3622-3640

Herrings Conyers and Kettel Charles (1951). On the theory of spin waves in ferromagnetic media. Physical Review, 81 (5): 869-879.

Halilov S.V., Perlov A.Ya., Oppeneer P.M., Yaresko A.N. and Antonov V.N. (1998). Magnetocrystalline anisotropy energy in cubic Fe, Co, and Ni: Applicability of local-spin-density theory reexamined. Physical Review B, 57 (16): 9557-9559

Haghiri-Gosnet A.M. and Renard J.P (2003). CMR manganites: Physics, Thin films, and Devices. Journal of Physics D: Applied Physics, 36: R127-R150

Heinrich B. and Bland J.A.C. Bland (Eds) (1994). Ferromagnetic Resonance in Ultrathin Magnetic Structures II. Springer.

Johnson M.T., Bloemen P.J.H., den Broeder F.J.A. and de Varies J. J. (1996). Magnetic anisotropy in metallic multilayers. Rep. Prog. Phys., 59

Jamet Mattieu, Wernsdorfer Wolfgang, Thirion Christophe, Dupuis V´eronique, Pérez Patrice Mélinon Alain and Mailly Dominique (2004). Magnetic anisotropy in single clusters. Physical Review B, 69.

Jiang San Ping (2008). Development of lanthanum strontium perovskite cathode materials of solid oxide fuel cells. J. Mater Sci, 43: 6799-6833

Jiang Jin Jie and Weber Ralph T. (2001). Elexsys E 500 User's Manuel: Basic Operations. Manuel Version 2.0, Software Version 2.1. Copyright © 2001 Bruker Instruments, Inc

Kittel Charles (1948). On the theory of ferromagnetic resonance absorption. Physical Review, 73 (2): 155-161

Kusov A. A, Jaswal S.S., and Shan Z.S. (1992). Shape anisotropy of magnetic multilayers. Physical Review B, 46(5)

Kamzin A.S., Rosenbaum V.L. and Ol'khovik L.P. (1998). Investigation of the magnetic structure of surface and volume of aluminium-substituted Sr-M type hexaferrites. JETP LETTERS, 67(10).

Kohmoto Osamu (2007). Ferromagnetic resonance of amorphous Fe wire. Materials Science and Engineering A: 449-451

Kim Joo-Hyung, Grishin Alexander M., Radamson Herry H. (2006). Properties of $La_{0.75}Sr_{0.25}MnO_3$ films grown on Si substrate with $Si_{1-x}Ge_x$ and $Si_{1-y}C_y$ buffer layers. Thin Solid Films, 515: 411-415

Larson P. and Mazin I.I. (2002). Calculation of magnetic energy in YCo_5. Journal of Magnetism and Magnetic Materials, 264: 7-13

Liu X., Zhou Y.Y. and Furdyna J.K. (2007). Angular dependence of spin wave resonances and surface spin pinning in ferromagnetic(Ga, Mn) As films. Physical Review B, 75: 195220

Liu H.L., Kuo M.X., Her J.L., Weng K.S., Wang L.M., Cheng S.L. and Lin J.G. (2005). Thickness-dependent optical properties of $La_{0.7}Sr_{0.3}MnO_3$ thin films. Journal of Applied Physics, 97: 113528

Matthews M., Jansen R., Rijnders G. R., Lodder J.C. and Blank D.H.A. (2009). Magnetic oxide nanowires with strain-controlled uniaxial magnetic anisotropy direction. Physical Review B, 80: 064408

Manabe T., Fujimoto T., Yamaguchi I., Kondo W., Kojima I., Mizuta S. and Kumagai T. (1998). Effects of substrate materials and annealing temperature on crystal structure and epitaxy of

Malinowski G., Kuiper K.C., Lavrijsen R., Swagten H.J.M. and Koopmans B. (2009). Magnetization dynamics and Gilbert damping in ultrathin $Co_{48}Fe_{23}B_{20}$ films with out-of-plane anisotropy. Applied Physics Letters, 94 (10).

Mosendz Oleksandre (2008). Magnetization Dynamics in Ultrathin Magnetic Films. Simon Fraser University. Phd thesis work.

McMichael R.D., Stiles M.D., Chen P.J. and Egelhoff W.F.Jr.,(1998). Ferromagnetic resonance linewidth in thin films coupled to NiO. Physical Review B, 58 (13)

McMichael R.D., and Krivosik Pavol (2004). Classical model of extrinsic ferromagnetic resonance linewidth in ultrathin films. IEEE TRANSACTIONS OF MAGNETICS, 40 (1)

Ma Chunlan, Yang Zhongqin and Picozzi Silvia (2006). Ab initio electronic and magnetic structure in $La_{0.66}Sr_{0.33}MnO_3$: strain and correlation effects. J. Phys.: Condens. Matter, 18: 7717-7728.

Nacher Pierre–Jean (2007). Magnetic Resonance Imaging: From Spin Physics to Medical Diagnosis.

Nalwa Hari Singh (2002). Handbook of Thin Film Materials. Academic Press.

Oogane Mikihiko, Wakitani Takeshi, Yakata Satoshi, Yilgin Resul, Ando Yasuo, Sakuma Akimasa and Miyazaki Terunobu (2006). Magnetic damping in ferromagnetic thin film. Japanese Journal of Applied Physics, 45 (5A): 3889-3891.

Patton. FMR linewidth measurement. Retrieved on 24/12/10 at http://www.mrc.uidaho.edu/em/Files/FMR_measurement.pdf

Phillips T.G. and Rosenberg H.M. (1966). Spin waves in ferromagnets. Rep. Prog. Phys: 286-329

Pandey B., Ghost S., Srivastava P., Avasthi D.K., Kabiraj D. and Pivin J.C. (2008). Synthesis and characterization of Ni-doped ZnO : A transparent magnetic semiconductor. Journal of Magnetism and Magnetic Materials, 320 : 3347-3351.

Petrakis Leonidas (2000). Spectra Line Shapes: Gaussian and Lorentzian functions in magnetic resonance. Journal of Chemical education

Poulopoulo P. and Baberschke K. (1999). Magnetism in thin films. J. Phys: Condens. Matter, 11.

Pradhan A.K., Dadson J.B., Hunter D., Zhang K., Mohanty S., Jackson E.M., Lasley–Hunter B., Lord K., Williams T.M., Rakhimov, Zhang J., Sellmyer D.J., Inaba K., Hasegawa T., Mathews S., Joseph B., Sekhar B.R., Roy U.N. Cui Y. and Burger A.(2006). Ferromagnetic properties of epitaxial manganite films on $SrTiO_3$/ Si heterostructures. Journal of Applied physics: 100(033903)

Rudd Jeffery MacLeod (1985). Ferromagnetic resonance in nickel at low temperatures. Master of Science Thesis. Simon Fraser University

Ruzmetov Dmirty, Seo Yongho, Belenky Land J., Kim D.M., Ke Xianglin, Sun Haipin, Chandrasekhar Venkat, Eom Chang-Beom, Rzchowski Mark S. and Pan Xiaoqing (2005). Epitaxial magnetic perovskite nanostructures. Advanced Materials: 1-15

Rickart M., MewesT., Demokritov S.O., Hillerbrands B. and Scheib M. (2004). Correlation between topography and magnetic surface anisotropy in epitaxial Fe films on vicinal-to-(001) Au surfaces with different step orientation. Physical Review B, 70.

Sankey, J.C., Braganca, P.M., Garcia, A.G.F., Krivorotov, I.N., Buhrman, R.A., and Ralph, D.C. (2006). Spin-transport-driven-ferromagnetic resonance of individual nanomagnets. Physical Review Letters. PRL 96: 227601..

Stancil Daniel D. and Prabhakar Anil (2009). Spin waves. Theory and Applications. Springer Science.

Stöhr J. and Siegmann H.C. (2006). Magnetism from Fundamental to Nanoscale Dynamics. Springer

Sharma Parmanand, Gupta Amita, RaO K.V., Owens Frank J. O, Sharma Renu, Ahuja Rajeev, Guillen Osorio J.M., Johansson Börje and Gehring G.A. (2003). Ferromagnetism above room temperature in bulk and transparent thin films of Mn-doped ZnO. Nature Materials, 2: 673-676.

S´trbik V., Spankora M., Reiffers M., Kovac J. and Benacka S. (2010). Transport and magnetic properties of epitaxial LSMO thin films grown on MgO single crystal substrates. Journal of Physics, Conference Series 233.

Stanescu Dana Elena Sorea (2004). Magnetization Dynamics in Magnetic Nanostructures. Phd thesis submitted to the Department of Physics, Joseph Fourier University.

Sellmyer David and Skomski Ralph (2006). Advanced Magnetic Nanostructures. Springer Science and Business Media Inc ; New York pp 67-68

Stoneham A.M. (1972). Linewidths with Gaussian and Lorentzian broadening. J. Phys. D: Appl. Physics, 5.

Srivastava Anul K., Hurben Michael J., Wittenauer Michael A., Kabos Pavel, Patton C. E., Ramesh R., Dorsy Paul C. and Chrisey Douglas B. (1999). Angle dependence of the ferromagnetic resonance linewidth and two magnon loses in pulsed deposited films of yttrium iron garnet, MnZn and NiZn ferrite. Journal of Applied Physics, 85(11).

Seo S.H., Jang H.C. and Noh D.Y. (2005). Effects of oxygen incorporation in tensile $La_{0.84}Sr_{0.16}MnO_3$. Physical Review B, 71: 012412.

Suzuki Y., Hwang H.Y., Cheong S.W. and Van Dover R.B (1997). The role of strain in metallic anisotropy of manganite thin films. Applied Physics Letters

Tanaka Kiyota, Okamura Soichiro and Shiosaki Tadashi (2001). Fabrication of perovskite manganite (La, Sr)MnO_3 thin films by chemical solution deposition and their low-field magnetoresistance properties at room temperature. Japanese Journal of Applied Physics. 40: 6821-6824.

Tserkovnyak Yaroslav, Brataas Arne, Bauer Gerrit E.W and Halperin Bertrand I. (2005). Nonlocal magnetization dynamics in ferromagnetic heterostructures. Review of Modern Physics, 77.

Tovsolytkin A., Pogorily A., Vovk A., Podyalovskii, Lezhnenko I., Marviyenko A., (2004). Magnetoresistance and phase separation in thin films of moderately Sr-doped manganites. Journal of Magnetism and Magnetic Materials, 272-276: 1839-1840

Uemura Tetsu, Sekine Kenji, Matsuba Ken-ichi and Yamamoto Masafumi (2005). Magnetic and Electrical Properties of (La;Sr)MnO_3 sputtered on $SrTiO_3$-Buffered Si Substrate. Japanese Journal of Applied Physics, 44(4B): pp 2604-2607

Urban R., Woltersdorf G. and Heinrich B. (2001). Gilbert damping in single and multilayer ultrathin films: Role of interfaces in nonlocal spin dynamics. Phys. Rev. Lett, 87 (21) :217204.

Witters J., Herlach F. and Bockstal L. Van. The FMR Linewidth of Iron-nickel alloys in high magnetic fields. Department of Physics. University of Leuven, Belgium. Retrieved on 24/12/10 at http://www.ismar.org/files/bulletin/BMR_08_184-187_1986.pdf

Wang Ding-sheng, Wu Ruqian and Freeman A.J. (1993). First principles theory of surface magnetocrystalline anisotropy and diatomic-pair model. Physical Review B, 47 (22)

Yilgin Resul, Oogane MIkihiko, Yakata Stoshi, Ando Yasuo and Miyazaki Terunobu (2005). Intrinsic Gilbert Damping Constant in Co_2MnAl Heusler Alloy Films. IEEE TRANSACTIONS ON MAGNETICS, 41(1)

7 APPENDICES

7.0 APPENDIX A

Data extracted from measurement on the EPR spectrometer for the 15 uc thick LSMO thin film at 150 K and 9.75 GHz**.**

Angle/^{o}	Field/Oe	Angle/^{o}	Field/Oe	Angle/^{o}	Field/Oe
1	1114.25	61	1093.25	121	925.00
2	1103.00	62	1092.25	122	929.75
3	1090.25	63	1088.75	123	937.25
4	1077.50	64	914.00	124	946.25
5	1063.00	65	917.00	125	957.25
6	1048.25	66	923.25	126	970.00
7	1033.25	67	923.50	127	951.00
8	1017.75	68	930.75	128	942.50
9	1002.00	69	1009.25	129	931.25
10	1111.0	70	1023.00	130	924.00
11	1120.25	71	1035.50	131	920.25
12	1129.00	72	1048.00	132	916.75
13	1134.25	73	914.00	133	913.75
14	1138.25	74	911.25	134	912.00
15	1607.50	75	910.00	135	913.50
16	1134.50	76	908.25	136	1081.00
17	1130.50	77	906.25	137	1070.00
18	1122.75	78	906.75	138	1060.50
19	984.25	79	907.50	139	1050.75
20	998.00	80	908.25	140	1039.25
21	1013.25	81	910.75	141	1024.75
22	1028.25	82	990.25	142	1012.25
23	1043.75	83	977.00	143	988.25
24	1059.75	84	962.75	144	976.50
25	1072.75	85	951.25	145	1058.50
26	1087.00	86	940.75	146	1068.75
27	1101.00	87	930.75	147	1076.25
28	916.25	88	924.25	148	1081.75
29	918.50	89	920.25	149	1084.50
30	922.00	90	916.00	150	1087.50
31	926.25	91	1116.25	151	1094.00
32	930.75	92	1104.75	152	1093.25
33	938.50	93	1092.00	153	1088.25

34	948.00	94	1079.50	154	987.50
35	958.75	95	1065.75	155	973.75
36	971.75	96	1050.25	156	960.25
37	952.25	97	1035.50	157	948.75
38	943.00	98	1020.50	158	938.00
39	930.50	99	1004.50	159	928.50
40	925.00	100	1110.00	160	922.25
41	920.75	101	1118.50	161	918.25
42	917.00	102	1126.50	162	914.50
43	914.75	103	1132.00	163	911.75
44	912.75	104	1134.75	164	909.75
45	914.25	105	1134.50	165	908.50
46	1081.75	106	1132.50	166	906.75
47	1070.25	107	1130.25	167	905.50
48	1062.00	108	1123.50	168	905.75
49	1051.50	109	982.25	169	906.50
50	1039.25	110	996.25	170	908.00
51	1026.00	111	1011.25	171	909.75
52	1012.50	112	1026.00	172	913.75
53	988.75	113	1041.25	173	917.25
54	977.00	114	1057.50	174	923.75
55	1057.75	115	1071.25	175	931.75
56	1068.50	116	1085.00	176	995.75
57	1074.75	117	1098.75	177	1011.75
58	1079.25	118	915.50	178	1024.00
59	1085.00	119	917.50	179	1034.75
60	1087.00	120	921.00	180	1049.00

7.1 APPENDIX B

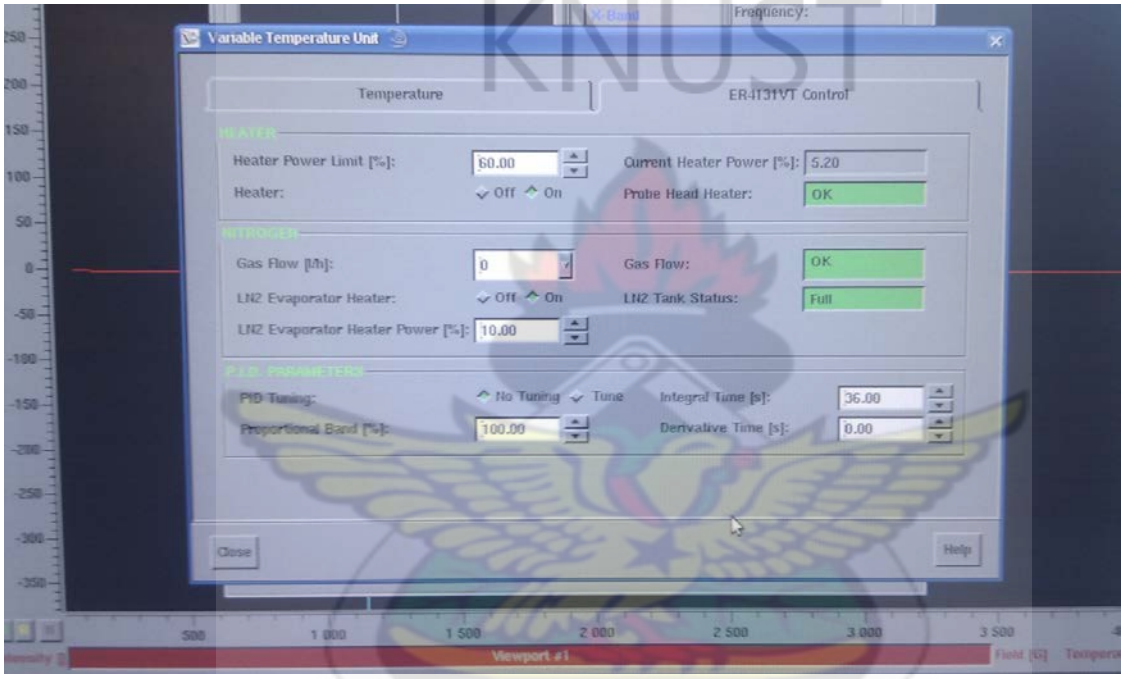

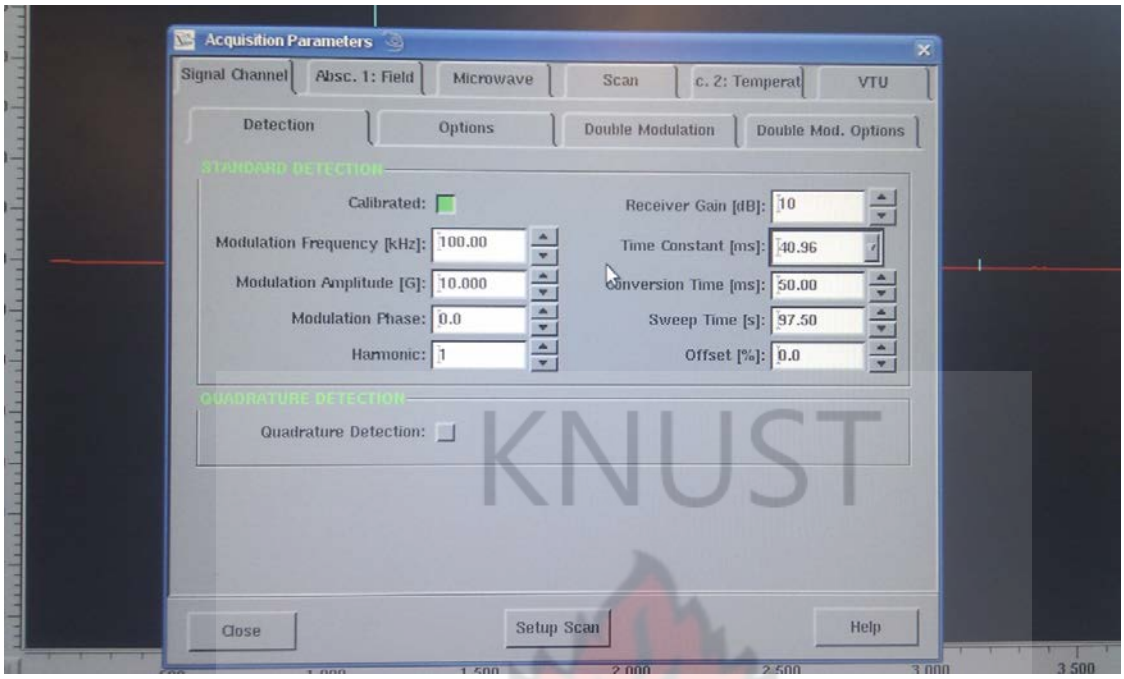
Acquisition Parameters
Signal Channel
Absc. 1: Field
Microwave
Scan
c. 2: Temperat
VTU
Detection
Options
Double Modulation
Double Mod. Options
STANDARD DETECTION
Calibrated:
Modulation Frequency [kHz]: 100.00
Modulation Amplitude [G]: 10.000
Modulation Phase: 0.0
Harmonic: 1
Receiver Gain [dB]: 10
Time Constant [ms]: 40.96
Conversion Time [ms]: 50.00
Sweep Time [s]: 97.50
Offset [%]: 0.0
QUADRATURE DETECTION
Quadrature Detection:
Close
Setup Scan
Help
1 000
1 500
2 000
2 500
3 000
3 500

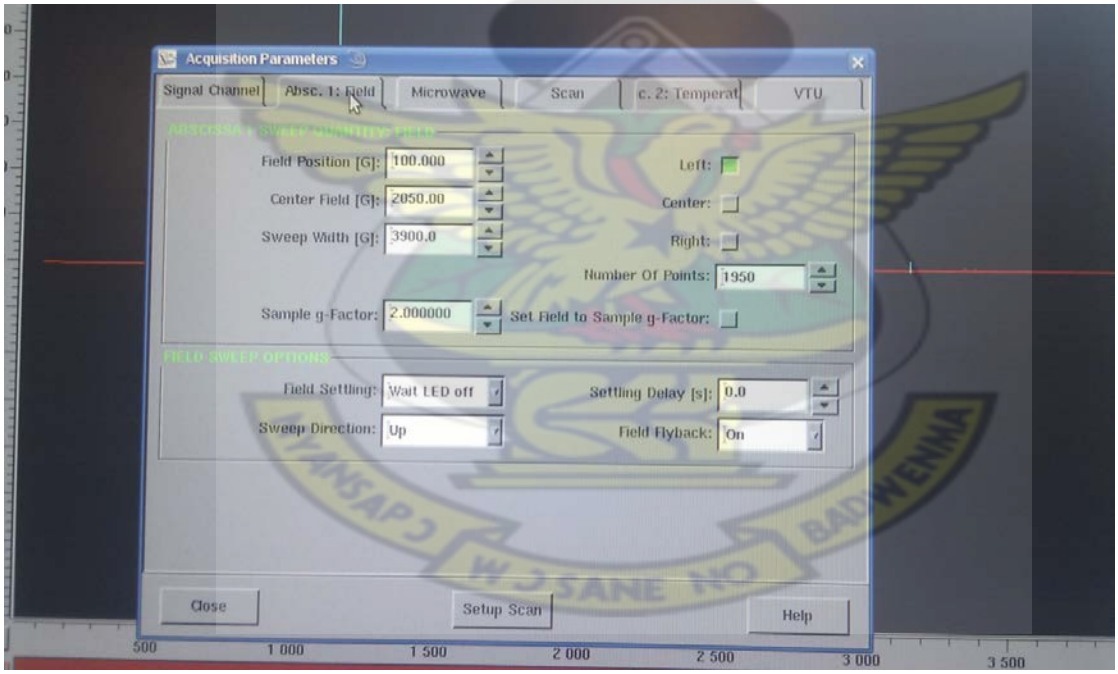
Acquisition Parameters
Signal Channel
Absc. 1: Field
Microwave
Scan
c. 2: Temperat
VTU
Field Position [G]: 100.000
Center Field [G]: 2050.00
Sweep Width [G]: 3900.0
Sample g-Factor: 2.000000
Left:
Center:
Right:
Number Of Points: 1950
Set Field to Sample g-Factor:
FIELD SWEEP OPTIONS
Field Settling: Wait LED off
Sweep Direction: Up
Settling Delay [s]: 0.0
Field Flyback: On
Close
Setup Scan
Help
500
1 000
1 500
2 000
2 500
3 000
3 500

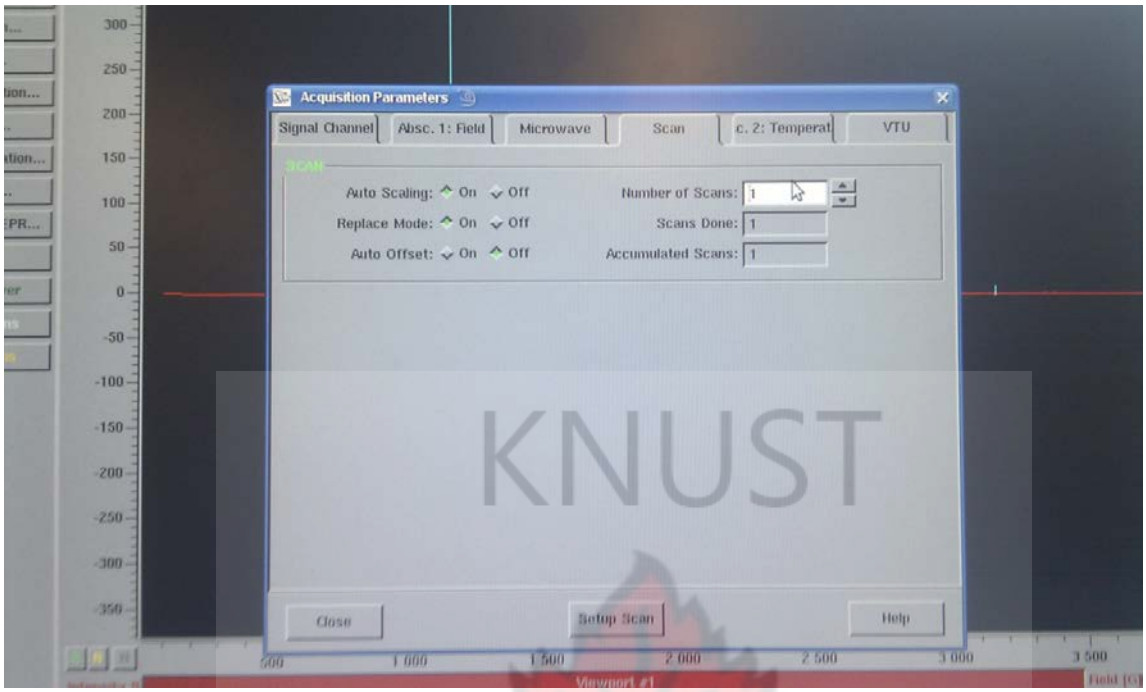
Acquisition Parameters
Signal Channel
Absc. 1: Field
Microwave
Scan
c. 2: Temperat
VTU
SCAN
Auto Scaling: On Off
Replace Mode: On Off
Auto Offset: On Off
Number of Scans: 1
Scans Done: 1
Accumulated Scans: 1
Close
Setup Scan
Help
Viewport #1

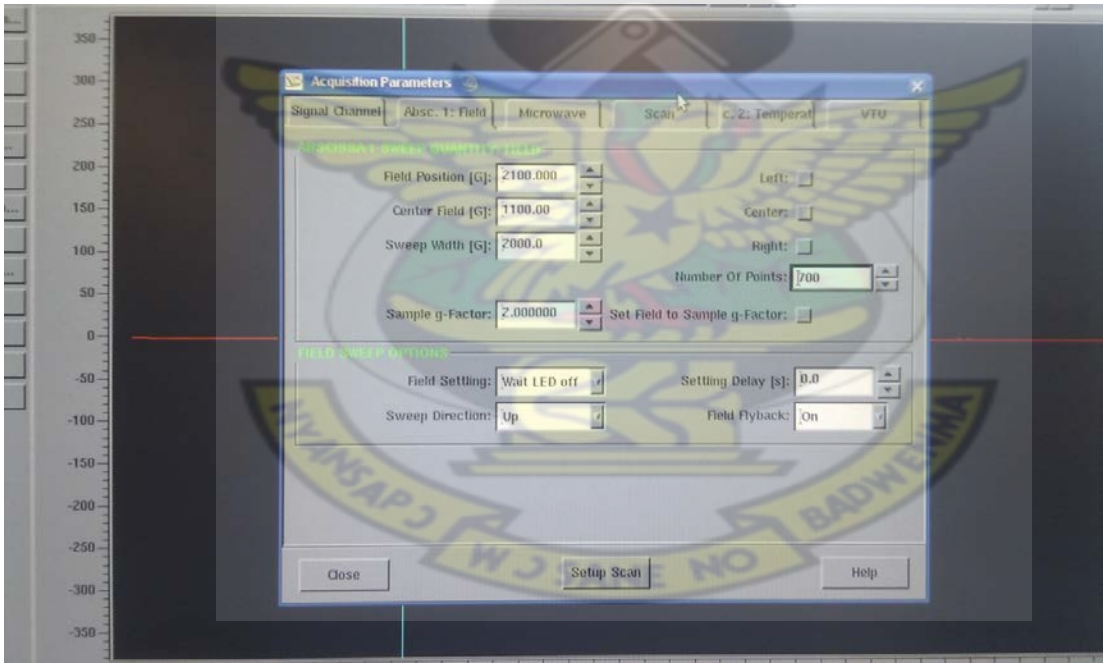
Acquisition Parameters
Signal Channel
Absc. 1: Field
Microwave
Scan
c. 2: Temperat
VTU
Field Position [G]: 2100.000
Center Field [G]: 1100.00
Sweep Width [G]: 2000.0
Left:
Center:
Right:
Number Of Points: 700
Sample g-Factor: 2.000000
Set Field to Sample g-Factor:
FIELD SWEEP OPTIONS
Field Settling: Wait LED off
Sweep Direction: Up
Settling Delay [s]: 0.0
Field Flyback: On
Close
Setup Scan
Help

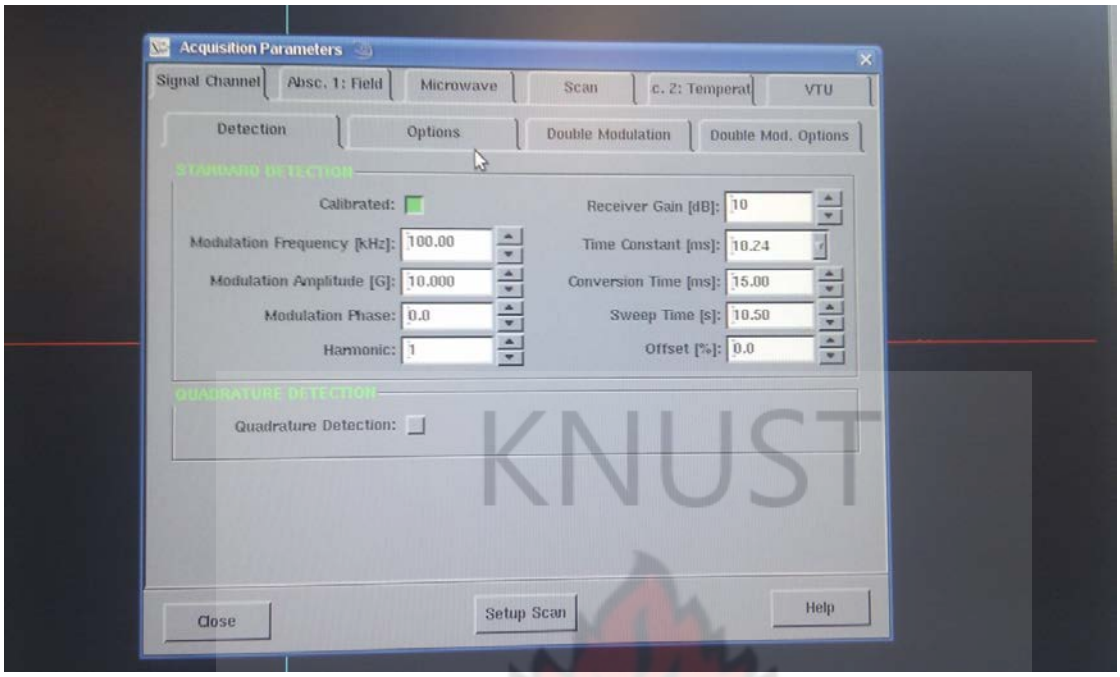

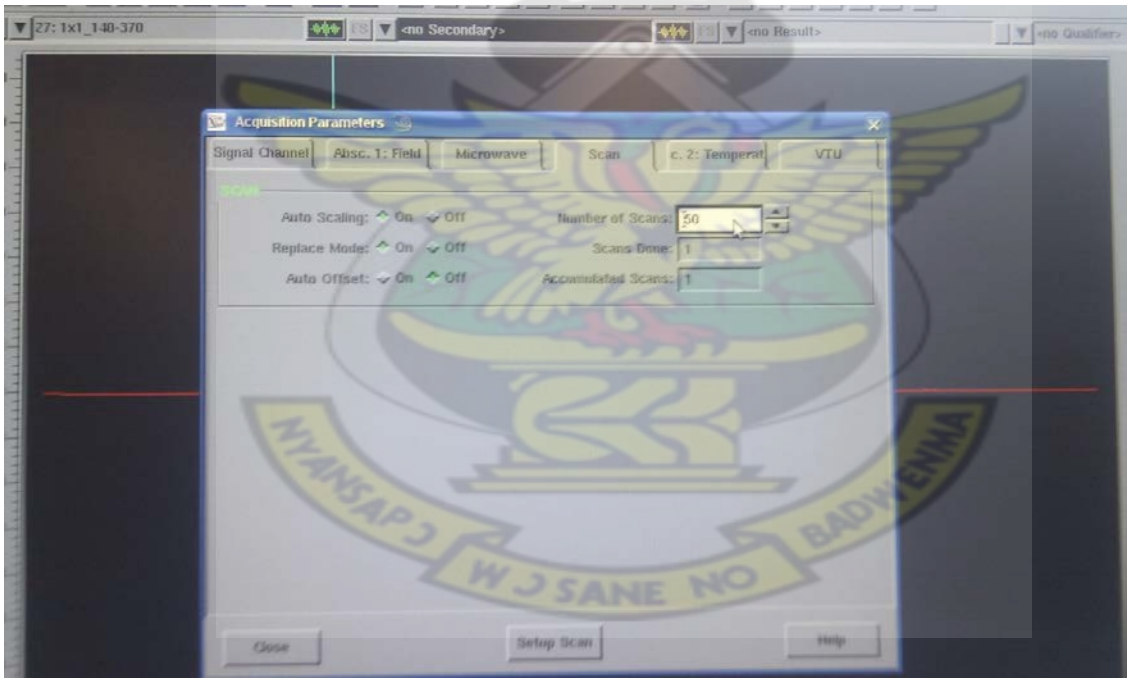

Some acquisition parameters observed on the EPR spectrometer

7.3 APPENDIX C

The setup of EPR spectrometer

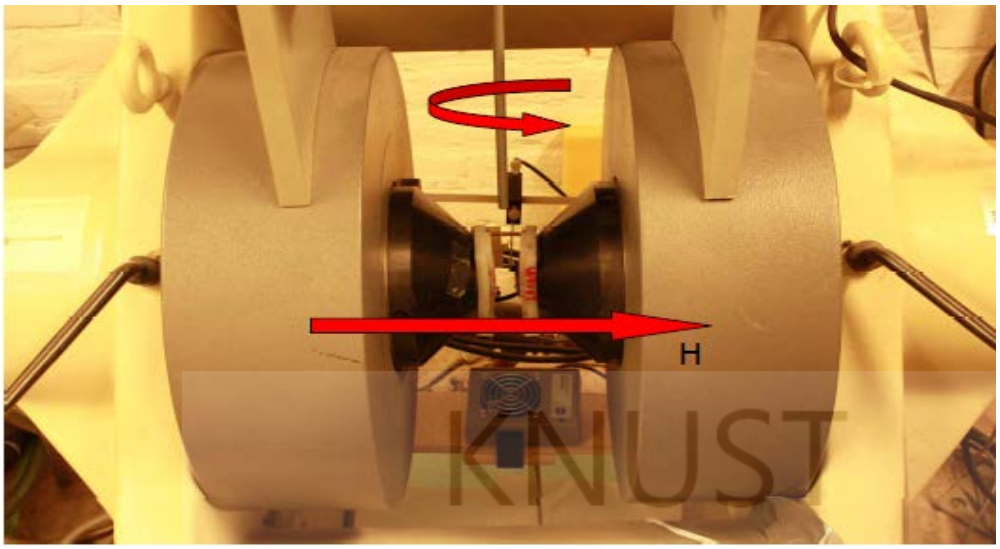

Spectrometer showing the direction of the applied field in the horizontal direction.

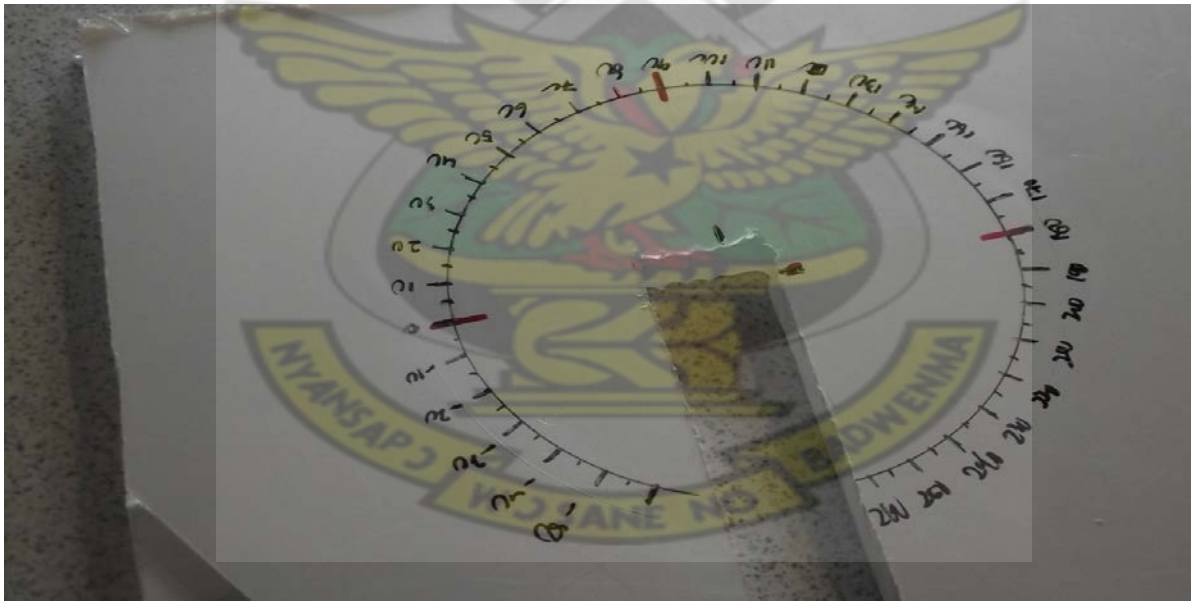

Rubber disk with calibration which is was inserted in the cavity of the spectrometer

for FMR measurement.

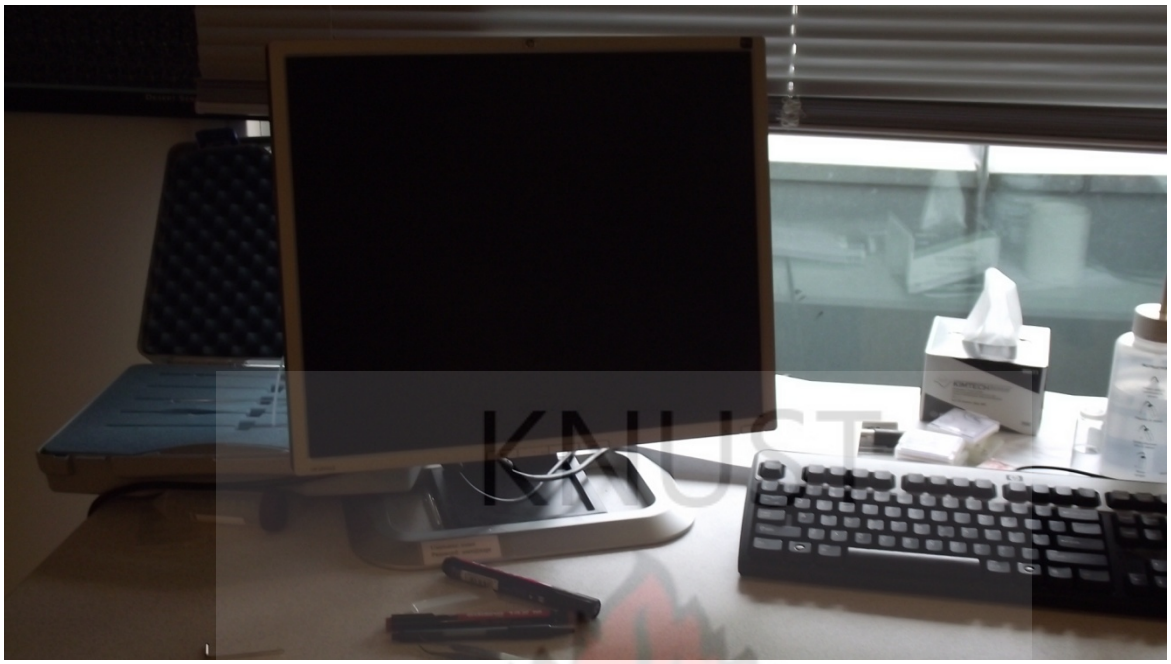

Personal computer for system control and for data acquisition.

7.4 APPENDIX D: MATLAB CODE

```
% Matlab code written by Godfred Inkoom.

% This code works only by installing first easyspin toolbox from http://easyspin.org/

%% Loading of data

clear all

clc

file_150=('C:\Users\Justice\Desktop\godfred\150K_rotation_complete_no_saturation.DTA');

file_200=('C:\Users\Justice\Desktop\godfred\200K_complete_roteation.DTA');

file_250=('C:\Users\Justice\Desktop\godfred\250K_rotation_complete.DTA');

[x,y,Params] = eprload(file_150);
```

```
[X,Y,Params1] = eprload(file_200);

[x0,y0,Params2] = eprload(file_250);

 x1=1:1:180; X1=1:1:180;x01=1:1:180;

%

z=y; Z=Y;  z0=y0;

 %% Surface plots

figure; mesh(x1,x{1},z); xlim([0 180]) ;xlabel('Angle'); ylabel('Field');zlabel('Signal');

figure; mesh(X1,X{1},Z),  xlim([0 180]);xlabel('Angle'); ylabel('Field');zlabel('Signal');

figure; mesh(x01,x0{1},z0); xlim([0 180]);xlabel('Angle'); ylabel('Field');zlabel('Signal');

%% Plot of Signal vrs Angles.

figure; plot(x3,y(1,:)); xlabel('Angle'); ylabel('Recorded Signal');

figure; plot(x3,Y(1,:)); xlabel('Angle'); ylabel('Recorded Signal');

figure; plot(x3,y0(1,:));xlabel('Angle'); ylabel('Recorded Signal');

%% Signal vrs Field plots

figure

plot(x{1,1}(1,1:4800),y); xlabel('Field'); ylabel('Recorded signal')

figure

plot(X{1,1}(1,1:2700),Y);xlabel('Field'); ylabel('Recorded signal')

figure

plot(x0{1,1}(1,1:1800),y0);xlabel('Field'); ylabel('Recorded signal')

%% combine plots

figure

plot(x{1,1}(1,1:4800),y,'g');
```

```
hold on

plot(X{1,1}(1,1:2700),Y,'b');

hold on

plot(x0{1,1}(1,1:1800),y0,'r');xlabel('Field'); ylabel('Recorded signal')

hold off
```